Toward the excited meson spectrum of dynamical QCD

Jozef J. Dudek,[1,2,*] Robert G. Edwards,[1] Michael J. Peardon,[3] David G. Richards,[1] and
Christopher E. Thomas[1]

(for the Hadron Spectrum Collaboration)

[1]*Jefferson Laboratory, 12000 Jefferson Avenue, Newport News, Virginia 23606, USA*
[2]*Department of Physics, Old Dominion University, Norfolk, Virginia 23529, USA*
[3]*School of Mathematics, Trinity College, Dublin 2, Ireland*
(Received 29 April 2010; revised manuscript received 10 June 2010; published 12 August 2010)

We present a detailed description of the extraction of the highly excited isovector meson spectrum on dynamical anisotropic lattices using a new quark-field construction algorithm and a large variational basis of operators. With careful operator construction, the combination of these techniques is used to identify the continuum spin of extracted states reliably, overcoming the reduced rotational symmetry of the cubic lattice. Excited states, states with exotic quantum numbers (0^{+-}, 1^{-+} and 2^{+-}), and states of high spin are resolved, including, for the first time in a lattice QCD calculation, spin-four states. The determinations of the spectrum of isovector mesons and kaons are performed on dynamical lattices with two volumes and with pion masses down to ~400 MeV, with statistical precision typically at or below 1% even for highly excited states.

I. INTRODUCTION

Computing the bound states of QCD is vital if we are to claim a complete description of the strong interactions. Confronting high-precision calculations of the spectrum with future experimental measurements will test the theoretical framework for such a description rigorously. There has been a resurgence of interest in the experimental investigations of the spectrum, notably in the charmonium sector where a wealth of high-quality data from the *B*-factories has challenged our understanding of spectroscopy. A comprehensive investigation of the spectrum of mesons composed of light quarks is the goal of the GlueX collaboration, after the 12 GeV upgrade of Jefferson Laboratory. Here the aim is to photoproduce mesons, and, in particular, those with exotic quantum numbers, as a means of revealing the role of gluonic degrees of freedom in the spectrum. There are also plans to study such mesons elsewhere, for example, at the PANDA experiment at FAIR.

Lattice calculations offer a method of performing a first-principles computation of the spectrum of QCD, and the calculation of the masses of the lowest-lying states has been an important benchmark of lattice studies since their inception. However, recently there has been considerable progress aimed at extracting the spectrum of excited states, both for mesons and for baryons. This has been accomplished through the use of the variational method, employing a large basis of interpolating operators satisfying the symmetries allowed by the cubic lattice [1–4]. In a series of

recent papers, we have applied this methodology to the extraction of the meson spectrum [5], and the radiative transitions between excited and low-lying meson states [6,7]. The first studies were performed in the quenched approximation to QCD, for mesons composed of the heavier charm quark and its antiquark, a system which is computationally less demanding yet for which there is a wealth of high-quality experimental data. In this paper, we investigate the spectrum of mesons for quark masses below the strange quark mass, going down to pion masses of around 400 MeV, and expand on our earlier letter [8] focused on the spectrum of mesons in full QCD with three mass-degenerate quark flavors.

Several previous studies of the spectrum have focussed on obtaining precision results for ground-state masses through controlling systematic errors [9–12]. Others have aimed at extracting the masses of some of the excited states [13–19]. The extraction of excited state masses is more difficult owing to the decrease in the signal-to-noise ratio with increasing time as we move progressively higher in the spectrum. To circumvent this difficulty, we use anisotropic lattices, with finer temporal than spatial lattice spacing, enabling the behavior of the Euclidean-space correlation functions to be examined at small temporal separations.

The (hyper-) cubic lattice does not possess the full rotational symmetry of the continuum. Thus, in a lattice calculation, states at rest are classified not according to the spin (J, J_z), but rather according to the irreducible representations (irreps) of a cube; for states of higher spin, the different continuum degrees of freedom are distributed across several lattice irreps. In this study, we use a large

*dudek@jlab.org

basis of interpolating operators, decomposed into their lattice irreps, that enable us to explore all J^{PC} up to spin 4, except for the exotic 4^{+-}, with as many as 26 operators in a given symmetry channel. Our ability to calculate correlation functions efficiently for such a large basis of operators relies on a new method, "distillation"[20], for the construction of quark-antiquark operators, including those with nonlocal construction.

As the lattice spacing approaches zero, full rotational symmetry is restored and thus, in principle, the spins can be identified through the emergence of energy degeneracies between different irreps. The increasing density of states in each irrep as we rise in the spectrum makes the identification of such degeneracies a challenging task, and thus the assignment of the continuum spins has been a formidable barrier to the interpretation of lattice calculations. In this paper, we adopt a very different approach, in which by judiciously constructing operators so as to have a known continuum behavior, the spins of the excited states are determined and thus the barrier imposed by the reduced cubic symmetry of the lattice is overcome.

A particularly interesting class of mesons are those with exotic J^{PC}, such as the 1^{-+} channel. Extracting clean signals for even the lightest state with these quantum numbers has proven difficult [18,21–26], with statistical noise levels typically being significantly higher than for other states. There is also a requirement to determine that any such extracted state is, in fact, the exotic spin 1 and not a nonexotic 4^{-+} state which would live in the same lattice irreducible representation. We found that we can extract information about exotic state masses at the same level of precision as excited nonexotic states ($\lesssim 1\%$), with the spins clearly identified.

First results, exploiting the full panoply of anisotropic lattices, "distillation" for efficient computation of the interpolating operators, and the identification of the continuum spins, have been presented for the case of three degenerate "strange" quarks [8]; the spectrum of excited states, including those with high spin, was extracted with confidence.

In this paper, we expand on the earlier work (at $m_\pi \approx 700$ MeV) to include calculations in full QCD both with three degenerate flavors of quark, and with a strange quark and two light quarks ($N_f = 2 \oplus 1$), corresponding to pion masses $m_\pi \simeq (520, 440, 400)$ MeV. Furthermore, we perform calculations at two spatial volumes, enabling us to seek possible finite-volume effects, and potentially the presence of multihadron states in the calculated spectrum. Precise extraction of such states is required in order to carry out analyses of resonances in the manner suggested by Lüscher [27].

The structure of the paper is as follows. We begin in Section II by presenting details of the QCD gauge-field configurations to be used. We describe the technology of two-point correlator measurement using distillation on dynamical gauge-field configurations in Section III. In Section IV, the construction of a set of composite QCD operators suitable for use in the extraction of the meson spectrum is outlined, along with a description of the procedure used to make these operators transform irreducibly under the limited rotations allowed on a cubic lattice. In Section V, we present the methodology utilized to extract meson spectral information from correlation functions. Section VI discusses the possibility of using the information embedded in vacuum-operator-state matrix elements to determine the spin of a meson, overcoming ambiguities introduced by the reduced rotational symmetry of a cubic lattice. The stability of the extracted spectral quantities to changes in the details of the correlator analysis is considered in Section VII, where it is seen that we can extract results of considerable robustness. In Section VIII, we report meson spectrum results extracted from calculations at 4 pion masses and 2 different lattice volumes. Results for isovector mesons, kaons, and the connected part of $s\bar{s}$ ("strangeonium") are shown. Section IX considers the apparent absence of multiparticle states within our extracted spectra. Finally, in Section X, we summarize our observations and suggest future directions.

II. LATTICE GAUGE FIELDS

In Euclidean space, excited state correlation functions decay faster than the ground state, and at large times are swamped by the signals of lower states, thus complicating the resolution of excited states. To ameliorate this problem we have adopted a dynamical anisotropic lattice formulation whereby the temporal extent is discretized with a finer lattice spacing than in the spatial directions [28,29]; this has proven crucial to obtain the results shown in this paper. This method avoids the computational cost that would come from reducing the spacing in all directions. Improved gauge and fermion actions are used, corresponding to two light dynamical quarks and one strange dynamical quark. Details describing the formulation of the actions as well as the techniques used to determine the anisotropy parameters can be found in Refs. [28,29]. The lattices have a spatial lattice spacing $a_s \sim 0.12$ fm with a temporal lattice spacing 3.5 times smaller corresponding to a temporal scale $a_t^{-1} \sim 5.6$ GeV. The gauge fields are periodic in all directions while the quark inversions are periodic spatially and antiperiodic temporally.

Previous work [8] showed results using the three-flavor degenerate quark-mass data set corresponding to bare light and strange quark masses $a_t m_l = a_t m_s = -0.0743$ and lattice size $16^3 \times 128$. In this limit, the bare strange quark mass was determined by tuning the ratio of the kaon mass to Ω baryon mass to its physical value [29]. The pion mass (degenerate with the kaon and η masses) is roughly 700 MeV. In this work, results are extended to lighter masses $a_t m_l = (-0.0808, -0.0830, -0.0840)$ and $a_t m_s = -0.0743$ corresponding to $2 + 1$ flavors of dynamical

TABLE I. The lattice data sets and propagators used in this paper. The lattice size and number of configurations are listed, as well as the number of time sources and the number of distillation vectors N_{vecs}. The total number of inversions for each quark mass = $4 \times N_{t_{\text{srcs}}} \times N_{\text{vecs}} \times N_{\text{cfgs}}$ is shown.

	$\frac{m_\ell}{m_s}$	$m_\pi/$MeV	m_K/m_π	volume	N_{cfgs}	$N_{t_{\text{srcs}}}$	N_{vecs}	$N_{\text{inv}}/10^6$
_743_	$\begin{matrix}-0.0743\\-0.0743\end{matrix}$	702	1	$16^3 \times 128$	536	9	64	1.2
				$20^3 \times 128$	198	6	128	0.6
_808_	$\begin{matrix}-0.0808\\-0.0743\end{matrix}$	524	1.15	$16^3 \times 128$	500	7	64	0.9
				$20^3 \times 128$	382	4	96	0.6
_830_	$\begin{matrix}-0.0830\\-0.0743\end{matrix}$	444	1.29	$16^3 \times 128$	601	10	64	1.5
_840_	$\begin{matrix}-0.0840\\-0.0743\end{matrix}$	396	1.39	$16^3 \times 128$	479	32	64	3.9
				$20^3 \times 128$	600	6	128	1.8

quarks, and lattice sizes $16^3 \times 128$, as well as $20^3 \times 128$. The bare strange quark mass was held fixed to its tuned value of $a_t m_s = -0.0743$. These fully dynamical data sets, described in more detail in Table I, allow for some investigations of the quark-mass dependence as well as finite-volume dependence of the spectrum.

The lattice scale, quoted above, is determined in the physical quark-mass limit using the Ω baryon mass (denoted by $a_t m_\Omega$). As noted, these calculations are carried out away from this limit. To facilitate comparisons of the spectrum at different quark masses, the ratio of hadron masses with the Ω baryon mass is used to remove the explicit scale dependence [29].

III. CORRELATOR CONSTRUCTION

The determination of the excited spectrum proceeds from the calculation of correlation functions between a basis of Hermitian creation and annihilation operators $\mathcal{O}$ at Euclidean times 0 and t,

$$C_{ij}(t) = \langle 0|\mathcal{O}_i(t)\mathcal{O}_j(0)|0\rangle.$$

Inserting a complete set of eigenstates of the Hamiltonian, such that $\hat{H}|\mathfrak{n}\rangle = E_\mathfrak{n}|\mathfrak{n}\rangle$, this correlation function decomposes into a sum of contributions from all states in the spectrum with the same quantum numbers as the source operators,

$$C_{ij}(t) = \sum_\mathfrak{n} \frac{1}{2E_\mathfrak{n}} \langle 0|\mathcal{O}_i|\mathfrak{n}\rangle\langle\mathfrak{n}|\mathcal{O}_j|0\rangle e^{-E_\mathfrak{n} t},$$

where the discrete character of the spectrum follows because the calculation is performed in finite-volume. In order to measure energies of low-lying states, it is crucial to construct operators that overlap predominantly with light modes.

Smearing is a well-established means to improve operator overlap, whereby a smoothing function is applied to the quark fields used in the creation operators. This smoothing function should effectively remove noisy short-range modes which should not make a significant contribution to the low-energy correlation functions. The Jacobi method [30] uses the gauge-covariant–second-order–three-

dimensional lattice Laplacian operator

$$-\nabla_{xy}^2(t) = 6\delta_{xy} - \sum_{j=1}^{3}(\tilde{U}_j(x,t)\delta_{x+\hat{j},y}$$
$$+ \tilde{U}_j^\dagger(x-\hat{j},t)\delta_{x-\hat{j},y}),$$

where the gauge fields, $\tilde{U}$, may be constructed from an appropriate covariant gauge-field-smearing algorithm [31]. To suppress high-energy modes of ∇^2, this operator is exponentiated, $\exp(\sigma\nabla^2)$, with some smearing weight σ. The resulting smoothed operator is then applied to the quark fields ψ.

The suppression of the high-energy modes of the Jacobi smearing operator $\exp(\sigma\nabla^2)$ means that only a small number of modes contribute significantly to the construction of the smeared quark fields, $\tilde{\psi}$. As suggested in Ref. [20], this smearing function can be replaced with a low-rank approximation. The "distillation" operator defines a smearing function

$$\Box_{xy}(t) = \sum_{k=1}^{N} \xi_x^{(k)}(t)\xi_y^{(k)\dagger}(t), \tag{1}$$

where $\xi_x^{(k)}$ are a finite number, N, of eigenvectors of ∇^2 evaluated on the background of the spatial gauge-fields of time slice t, once the eigenvectors have been sorted by eigenvalue. This is the projection operator into the subspace spanned by these eigenmodes, so $\Box^2 = \Box$.

This smearing function is used in the construction of isovector meson operators of the form $\bar{\tilde{\psi}}\Gamma\tilde{\psi}$, where Γ acts in spin and color as well as coordinate space. Applying the distillation operator $\Box$ onto each quark field, $\tilde{\psi} \equiv \Box\psi$, the creation operators at zero three-momentum are written as

$$\mathcal{O}_i(t) = \bar{\psi}_x(t)\Box_{xy}(t) \cdot \Gamma_{yz}^i(t) \cdot \Box_{zw}(t)\psi_w(t),$$

where there is an implied volume summation over repeated spatial indices. In a shorthand notation, the correlation function can be written as

$$C_{ij}(t) = \langle \bar{\psi}_t\Box_t\Gamma_t^i\Box_t\psi_t \cdot \bar{\psi}_0\Box_0\Gamma_0^j\Box_0\psi_0\rangle.$$

After evaluating the quark-field path-integral and inserting

the outer-product definition of the distillation operator $\square$ from Eq. (1), the correlator can be written

$$C_{ij}(t) = \text{Tr}[\Phi^j(t)\tau(t,0)\Phi^i(0)\tau(0,t)],$$

where

$$\Phi^i_{\alpha\beta}(0) = \xi^\dagger(0)[\mathbf{\Gamma}^i(0)]_{\alpha\beta}\xi(0),$$

encodes the structure of the operator and

$$\tau_{\alpha\beta}(t,0) = \xi^\dagger(t)M^{-1}_{\alpha\beta}(t,0)\xi(0),$$

is the "perambulator", with M the lattice representation of the Dirac operator, and where the quark spin indices, α, β of Φ and τ have been explicitly written. Φ has a well-defined momentum, while there is no explicit momentum projection in the definition of τ. The Φ and τ are square matrices of dimension NN_σ where $N_\sigma = 4$ are the number of spin components in a lattice Dirac spinor. Construction of the τ requires NN_σ inversions of the fermion matrix to compute all elements. These matrices are small compared to the dimension of the space of quark fields. Once the τ have been computed and stored, the correlation of any source and sink operators can be computed *a posteriori*. The method straightforwardly extends to the determination of multihadron two-point correlation functions [32] as well as three-point functions [20].

IV. CONSTRUCTION OF MESON OPERATORS

Meson spectral information will follow from analysis of two-point correlators featuring a large basis of composite QCD operators having mesonic quantum numbers. The simplest such operators are color-singlet local fermion bilinears, $\bar{\psi}_{i\alpha}(\vec{x},t)\Gamma_{\alpha\beta}\psi_{i\beta}(\vec{x},t)$, where the quantum numbers are determined by the choice of gamma matrix, Γ. In distillation [20], the quark fields ψ are replaced by the smeared quark fields $\tilde{\psi}$, but the rotationally symmetric nature of the smearing does not change the quantum numbers of the bilinear operators. These simple local operators are extremely limited in that they allow access only to the set $J^{PC} = 0^{-+}, 0^{++}, 1^{--}, 1^{++}, 1^{+-}$, and they do not offer significant redundancy within any J^{PC}. In order to consider higher spins, exotic J^{PC}, and to produce multiple operators within a given symmetry channel, one must consider extending to the use of nonlocal operators [13–18]. Our approach is to use spatially-directed–gauge-covariant derivatives within a fermion bilinear, that is to construct operators of essential structure

$$\sum_{\vec{x}} \bar{\psi}(\vec{x},t)\Gamma\vec{D}_i\vec{D}_j\ldots\psi(\vec{x},t)$$

where $\vec{D} \equiv \overleftarrow{D} - \overrightarrow{D}$ and where spin and color indices are suppressed for clarity. The use of the "forward-backward" derivative, $\vec{D}$, is not strictly necessary at zero momentum (projected by the sum over spatial sites), the only case we consider here, but it does somewhat simplify the construc-

tion of eigenoperators of charge conjugation as will be discussed below.

With the continuum $SO(3)$ rotational symmetry it is straightforward to produce operators of this type that are of definite spin, parity and charge conjugation at zero momentum. This follows from forming a circular basis of the Cartesian vectorlike derivatives and gamma matrices, $\vec{D}_i, \gamma_i, \gamma_5\gamma_i, \gamma_0\gamma_i, \epsilon_{ijk}\gamma_j\gamma_k$, e.g.,

$$\vec{D}_{m=-1} = \frac{i}{\sqrt{2}}(\vec{D}_x - i\vec{D}_y) \qquad \vec{D}_{m=0} = i\vec{D}_z$$

$$\vec{D}_{m=+1} = -\frac{i}{\sqrt{2}}(\vec{D}_x + i\vec{D}_y).$$

Once expressed in this basis, which transforms like spin-1, operators of definite spin can be constructed using the standard $SO(3)$ Clebsch-Gordan coefficients. For example, with a vectorlike gamma matrix and one covariant derivative, operators of $J = 0, 1, 2$ can be formed

$$(\Gamma \times D^{[1]}_{J=1})^{J,M} = \sum_{m_1, m_2} \langle 1, m_1; 1, m_2 | J, M \rangle \bar{\psi}\Gamma_{m_1}\vec{D}_{m_2}\psi.$$

The choice of Γ plays a role in setting the parity and charge-conjugation quantum numbers of the operator—our naming scheme for these matrices is given in Table II.

At the two-derivative level we adopt the convention of first coupling the two derivatives to a definite spin, J_D, then coupling with the vectorlike gamma matrix (if any) as

$$(\Gamma \times D^{[2]}_{J_D})^{J,M} = \sum_{m_1, m_2, m_3, m_D} \langle 1, m_3; J_D, m_D | J, M \rangle$$
$$\times \langle 1, m_1; 1, m_2 | J_D, m_D \rangle \bar{\psi}\Gamma_{m_3}\vec{D}_{m_1}\vec{D}_{m_2}\psi.$$

It is worth noting here that while the Clebsch-Gordan for $1 \otimes 1 \rightarrow 1$ is antisymmetric and $\vec{D}_{m_1}\vec{D}_{m_2}$ appears to be symmetric, there are nonzero operators with $J_D = 1$ because the gauge-covariant derivatives do not commute with each other in QCD. Rather these "commutator" operators are proportional to the gluonic field-strength tensor which does not vanish on nontrivial gluonic field configurations.

At the three-derivative level, we need to choose a convention for the ordering in which we couple the derivatives. A natural choice comes from insisting the operators have definite charge-conjugation symmetry. By exchanging the quark and antiquark fields, the charge-conjugation operation effectively acts as a transpose of the operators between the quark fields—for three derivatives then, one ensures definite charge conjugation by coupling the outermost derivatives together first since this gives them a definite exchange symmetry (even for $J_{13} = 0, 2$, odd for $J_{13} = 1$).

TABLE II.   Gamma matrix naming scheme.

	a_0	π	π_2	b_0	ρ	ρ_2	a_1	b_1
Γ	1	γ_5	$\gamma_0\gamma_5$	γ_0	γ_i	$\gamma_i\gamma_0$	$\gamma_5\gamma_i$	$\gamma_i\gamma_j$

This simple formulation is possible because we have used the forward-backward derivatives, $\overleftrightarrow{D}$.

$$(\Gamma \times D^{[3]}_{J_{13},J_D})^{J,M} = \sum_{m_1,m_2,m_3,m_4,m_{13},m_D} \langle 1, m_4; J_D, m_D | J, M \rangle$$
$$\times \langle 1, m_2; J_{13}, m_{13} | J_D, m_D \rangle$$
$$\times \langle 1, m_1; 1, m_3 | J_{13}, m_{13} \rangle$$
$$\times \bar{\psi} \Gamma_{m_4} \overleftrightarrow{D}_{m_1} \overleftrightarrow{D}_{m_2} \overleftrightarrow{D}_{m_3} \psi.$$

Clearly this procedure can be extended to as many covariant derivatives as one wishes. In this paper, we will use operators with up to three derivatives providing access to all J^{PC} with $J \leq 4$.[1]

The operators as formed are eigenstates of parity: when there are an even (odd) number of covariant derivatives, the parity is equal to (opposite to) that of the local operator containing the same gamma matrix. The operators are also eigenstates of charge-conjugation in the case that the ψ and $\bar{\psi}$ fields are of the same flavor. In the case that the fields are degenerate but not identical (e.g., the u and d quarks in our calculation), the C-parity is trivially generalized to G-parity. For kaons, where the light and strange quarks are not degenerate, there is no C-parity or any generalization of it. In this case, the symmetry channels are labeled by J^P and operators of both C can be used.

Subduction into lattice irreps

In lattice QCD calculations, the theory is discretized on a four-dimensional hypercubic Euclidean grid. The full three-dimensional rotational symmetry that classifies energy eigenstates in the continuum is hence reduced to the symmetry group of a cube (the cubic symmetry group, or equivalently the octahedral group). Instead of the infinite number of irreducible representations labeled by spin J, the single-cover cubic group relevant for integer spin has only five irreducible representations (*irreps*): A_1, T_1, T_2, E, A_2. The distribution of the various M components of a spin-J meson into the lattice irreps is known as *subduction*, the result of which is shown in Table III.

To be of any use in lattice computations, the continuum operators described above must be subduced into lattice irreps. Noting that each class of operator is closed under rotations, the subductions can be performed using known linear combinations of the M components for each J:

$$\mathcal{O}^{[J]}_{\Lambda,\lambda} \equiv (\Gamma \times D^{[n_D]}_{...})^{J}_{\Lambda,\lambda} = \sum_M \mathcal{S}^{J,M}_{\Lambda,\lambda} (\Gamma \times D^{[n_D]}_{...})^{J,M}$$

$$\equiv \sum_M \mathcal{S}^{J,M}_{\Lambda,\lambda} \mathcal{O}^{J,M},$$

where λ is the "row" of the irrep $(1 \ldots \dim(\Lambda))$. Note that, although $\mathcal{O}^{[J]}_{\Lambda,\lambda}$ can have an overlap with all spins contained

---

[1]Except the exotic 4^{+-}, which requires a minimum of four derivatives.

TABLE III. Continuum spins subduced into lattice irreps $\Lambda(\dim)$.

J	irreps
0	$A_1(1)$
1	$T_1(3)$
2	$T_2(3) \oplus E(2)$
3	$T_1(3) \oplus T_2(3) \oplus A_2(1)$
4	$A_1(1) \oplus T_1(3) \oplus T_2(3) \oplus E(2)$

within Λ (as listed in Table III for $J \leq 4$) it still carries the memory of the J from which it was subduced, a feature we exploit in Section VI. The subduction coefficients, $\mathcal{S}^{J,M}_{\Lambda,\lambda}$, form an orthogonal matrix, $\sum_M \mathcal{S}^{J,M}_{\Lambda,\lambda} \mathcal{S}^{J,M*}_{\Lambda',\lambda'} = \delta_{\Lambda,\Lambda'} \delta_{\lambda,\lambda'}$, and this fixes their normalization.

The subduction coefficients can be constructed in a number of different ways and here we give a simple derivation. More details and an alternative method using a group-theoretic projection formula can be found in Appendix A.

The simplest case is the subduction of the $J = 0$ operator; from Table III, this only subduces into the A_1 irrep and so trivially we have $\mathcal{S}^{0,0}_{A_1,1} = 1$. The $J = 1$ operator is also relatively straightforward, only subducing into the T_1 irrep with subduction coefficients shown in Appendix A. Note that $\mathcal{S}^{1,M}_{T_1,\lambda} = \delta_{\lambda,2-M}$, where the shift by 2 places λ in the range $1 \ldots \dim(\Lambda)$.

Subduction coefficients for all higher spins can be constructed by iteration, starting from the $J = 0$ and $J = 1$ coefficients and using

$$\mathcal{S}^{J,M}_{\Lambda,\lambda} = N \sum_{\lambda_1,\lambda_2} \sum_{M_1,M_2} \mathcal{S}^{J_1,M_1}_{\Lambda_1,\lambda_1} \mathcal{S}^{J_2,M_2}_{\Lambda_2,\lambda_2} C\begin{pmatrix} \Lambda & \Lambda_1 & \Lambda_2 \\ \lambda & \lambda_1 & \lambda_2 \end{pmatrix}$$
$$\times \langle J_1, M_1; J_2, M_2 | J, M \rangle.$$

Here $\langle J_1, M_1; J_2, M_2 | J, M \rangle$ is the usual $SO(3)$ Clebsch-Gordan coefficient for $J_1 \otimes J_2 \rightarrow J$ and

$$C\begin{pmatrix} \Lambda & \Lambda_1 & \Lambda_2 \\ \lambda & \lambda_1 & \lambda_2 \end{pmatrix}$$

is the octahedral group Clebsch-Gordan coefficient for $\Lambda_1 \otimes \Lambda_2 \rightarrow \Lambda$. N is a normalization factor, fixed by the requirement that the subduction coefficients form an orthogonal matrix as discussed above. We give explicit values for the subduction coefficients up to $J = 4$ in Appendix A.

In Table IV we show the number of operators we have in each lattice irrep, i.e., using all operators with up to 3 derivatives. We have performed extensive tests of this operator set to check that two-point correlators having operators in differing irreps at source and sink are consistent with zero and that similarly within an irrep, correlators of differing rows at source and sink are consistent with

TABLE IV. Number of distinct operators in each lattice irrep Λ^{PC}, using all operators with up to three derivatives. Each operator has $\dim(\Lambda)$ "rows".

A_1^{++}	13	A_1^{+-}	5	A_1^{-+}	12	A_1^{--}	6
T_1^{++}	22	T_1^{+-}	22	T_1^{-+}	18	T_1^{--}	26
T_2^{++}	22	T_2^{+-}	14	T_2^{-+}	18	T_2^{--}	18
E^{++}	17	E^{+-}	9	E^{-+}	14	E^{--}	12
A_2^{++}	5	A_2^{+-}	5	A_2^{-+}	4	A_2^{--}	6

zero. All such "orthogonality tests" are passed in explicit calculation.

For our final spectral extractions, we form a correlator matrix in a given irrep Λ and average over equivalent rows, λ,

$$C_{ij}^{\Lambda} \equiv \frac{1}{\dim(\Lambda)} \sum_{\lambda=1}^{\dim(\Lambda)} C_{i\lambda,j\lambda}^{\Lambda}$$

$$\equiv \frac{1}{\dim(\Lambda)} \sum_{\lambda} \langle 0 | \mathcal{O}_{i(\Lambda)\lambda}^{[J]} \mathcal{O}_{j(\Lambda)\lambda}^{[J]} | 0 \rangle,$$

where i, j labels the different operator constructions within the irrep Λ.

V. CORRELATOR ANALYSIS

The variational method for spectral extraction [33–35], which takes advantage of a redundancy of operators within a given symmetry channel, is now in common usage [5,13,15–17]. This method finds the best (in a variational sense) linear combination of operators within a finite basis for each state in the spectrum. Mathematically, it boils down to the solution of a linear system of generalized eigenvalue type:

$$C(t)v^{\mathfrak{n}}(t) = \lambda_{\mathfrak{n}}(t)C(t_0)v^{\mathfrak{n}}(t) \qquad (2)$$

where $\lambda_{\mathfrak{n}}(t_0) = 1$ and where there is an orthogonality condition on the eigenvectors of different states $(\mathfrak{n}, \mathfrak{n}')$, $v^{\mathfrak{n}'\dagger}C(t_0)v^{\mathfrak{n}} = \delta_{\mathfrak{n},\mathfrak{n}'}$. As discussed in Ref. [5], this orthogonality condition is very powerful in extracting near degenerate states which would be difficult to distinguish by their time dependence alone.

In our particular implementation of this method, Eq. (2) is solved for eigenvalues $\lambda_{\mathfrak{n}}$ and eigenvectors $v^{\mathfrak{n}}$, independently on each time slice, t. Ensuring the same ordering of states between time slices requires some care owing to the high degree of mass degeneracy in the meson spectrum. Rather than the obvious ordering by size of eigenvalue which might fluctuate time-slice by time-slice for nearby masses, we associate states between time slices using the similarity of their eigenvectors. We choose a reference time slice on which reference eigenvectors are defined, $v_{\text{ref}}^{\mathfrak{n}} \equiv v^{\mathfrak{n}}(t_{\text{ref}})$, and compare eigenvectors on other time slices by finding the maximum value of $v_{\text{ref}}^{\mathfrak{n}'\dagger}C(t_0)v^{\mathfrak{n}}$ which associates a state $\mathfrak{n}$ with a reference state $\mathfrak{n}'$. Using this

procedure, we observe essentially no "flipping" between states in either the principal correlators, $\lambda_{\mathfrak{n}}(t)$ or the eigenvectors $v^{\mathfrak{n}}(t)$, as functions of t.

Within finite-volume field theory, which has only discrete eigenstates, any two-point correlator can be expressed as a spectral decomposition,

$$C_{ij}(t) = \sum_{\mathfrak{n}} \frac{Z_i^{\mathfrak{n}*} Z_j^{\mathfrak{n}}}{2m_{\mathfrak{n}}} e^{-m_{\mathfrak{n}}t}, \qquad (3)$$

where this is an approximation valid providing $t \ll L_t$, the temporal length of the box. The "overlap factors", $Z_i^{\mathfrak{n}} \equiv \langle \mathfrak{n} | \mathcal{O}_i | 0 \rangle$ are related to the eigenvectors by $Z_i^{\mathfrak{n}} = \sqrt{2m_{\mathfrak{n}}} e^{m_{\mathfrak{n}}t_0/2} v_j^{\mathfrak{n}*} C_{ji}(t_0)$. The state masses follow from fitting the principal correlators, $\lambda_{\mathfrak{n}}(t)$, which for large times should tend to $e^{-m_{\mathfrak{n}}(t-t_0)}$. In practice we allow a second exponential in the fit form and use even relatively low time slices in order to stabilize the fit. The fit function is

$$\lambda_{\mathfrak{n}}(t) = (1 - A_{\mathfrak{n}})e^{-m_{\mathfrak{n}}(t-t_0)} + A_{\mathfrak{n}}e^{-m'_{\mathfrak{n}}(t-t_0)}, \qquad (4)$$

where the fit parameters are $m_{\mathfrak{n}}$, $m'_{\mathfrak{n}}$ and $A_{\mathfrak{n}}$. Typical fits for a set of excited states within an irrep are shown in Fig. 1 where we plot the principal correlator with the dominant
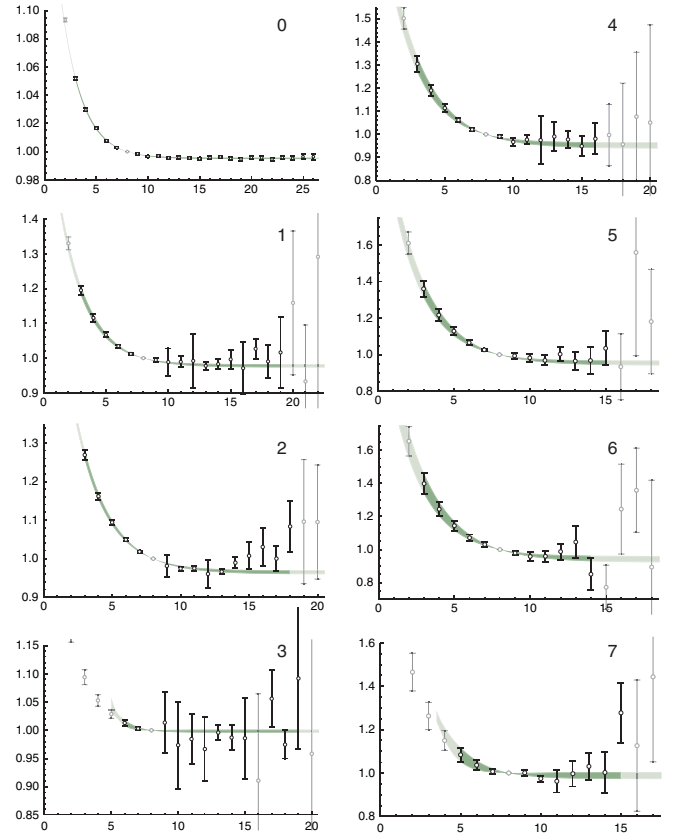

FIG. 1 (color online). Principal correlator fits according to Eq. (4). Eight states from the T_1^{--} irrep $(743, 16^3)$. Plotted are $\lambda^{\mathfrak{n}}(t) \cdot e^{m_{\mathfrak{n}}(t-t_0)}$ data and the fit for $t_0 = 8$. Data used in the fit are shown in black, while points excluded from the fit are in grey.

time-dependence due to state $\mathfrak{n}$ divided out. In such a plot one would see a horizontal line of value 1.0 in the case that a single exponential dominates the fit and clearly the data shows flat behavior for $t > t_0$.

Empirically we find that the size of the second exponential term decreases rapidly as one increases t_0. Further, we find, in agreement with the perturbative analysis of Ref. [35], that for large t_0 values the $m'_{\mathfrak{n}}$ extracted are larger than the value of $m_{\mathfrak{n}=\dim(C)}$, the largest "first" exponential mass extracted. At smaller t_0 values, this is not necessarily true and is indicative of forcing an incorrect orthogonality as discussed below. The values of $A_{\mathfrak{n}}$ and $m'_{\mathfrak{n}}$ are not used elsewhere in the analysis.

From the spectral decomposition of the correlator, Eq. (3), it is clear that there should in fact be no time dependence in the eigenvectors, while our independent solution of the generalized eigenvalue problem as a function of t has allowed there to be. The time-independent overlap factors, $Z_i^{\mathfrak{n}}$, which will be used later to identify the spin of extracted states, follow from fitting the $Z_i^{\mathfrak{n}}(t)$, obtained from the eigenvectors, with a constant or a constant plus an exponential (in the spirit of the perturbative corrections outlined in [35]).

The importance of choosing an appropriately large value of t_0 was emphasized in Ref. [5]. In this paper, we will follow the "reconstruction" scheme outlined therein in the selection of t_0. In short, the masses, $m_{\mathfrak{n}}$, extracted from fits to the principal correlators and the $Z_i^{\mathfrak{n}}$ extracted from the eigenvectors on a single time slice are used in Eq. (3) to "reconstruct" the correlator matrix. This reconstructed matrix is compared to the original data for all $t > t_0$, with the degree of agreement indicating the acceptability of the spectral description. The description generally improves as one increases t_0 until at some point the increase in statistical noise prevents further improvement. In particular, see Fig. 6 in Ref. [5], where the effect of choosing t_0 too small is clearly seen. Forcing the $\dim(C)$-state orthogonality, $v^{\mathfrak{m}\dagger} C(t_0) v^{\mathfrak{n}} = \delta_{\mathfrak{n},\mathfrak{m}}$, in a situation where accurate description of $C(t_0)$ requires more than $\dim(C)$ states leads to a poor description of the correlator matrix at times $t > t_0$. The reconstruction procedure gives a guide to the minimal t_0 for which the correlator matrix is well described by the variational solution. The sensitivity of extracted spectral quantities to the value of t_0 used will be discussed in detail in Sec. VII A, but in short it is usually necessary for us to use $t_0 \gtrsim 7$.

The RECONFIT2 code used for variational analysis is available within the ADAT suite [36].

VI. DETERMINING THE SPIN OF A STATE

In principle, the most rigorous method to determine the spin of a state is to perform the extraction of the spectrum for each lattice irrep at successively finer lattice spacings, and then to extrapolate the energies in each irrep to the continuum limit. There, one expects to see degeneracies

emerge according to the pattern of subduction, free of splittings arising from the discretization effects. Thus, for example, a spin-3 state would appear as degenerate energies within the A_2, T_1, and T_2 irreps. This procedure has been successfully applied to identify a number of low-lying states in the calculation of the glueball spectrum within pure $SU(3)$ Yang-Mills theory [37].

There are two reasons why this technique is not currently practical for the QCD meson spectrum. First, the procedure relies on a series of calculations on progressively finer lattices, and hence at increasing computational cost. Second, the continuum spectrum, classified according to the continuum quantum numbers, exhibits a high degree of degeneracy; when classified according to the symmetries of the cube, the degree of degeneracy is vastly magnified. Identification of degeneracies between irreps would require a statistical precision far beyond even that of the high-quality data presented here, as seen in Fig. 10 and subsequent figures.

To alleviate these difficulties, it would be useful to have a spin-identification method that is effective when using data obtained at only a single lattice spacing. Obviously, this lattice spacing should be fine enough that rotation symmetry has been restored to a sufficient degree in order that it be describing QCD. The mass degeneracy complications outlined above suggest that any alternative method needs to use state information beyond just the mass. Our suggestion is to consider the values of the vacuum-to-state matrix elements, or "overlaps" ($\langle \mathfrak{n}|\mathcal{O}|0\rangle$) of our carefully constructed subduced operators.

The operators constructed in Section IV transform irreducibly under the allowed cubic rotations, that is, they faithfully respect the symmetries of the lattice. However, it is also clear from the method of construction that each
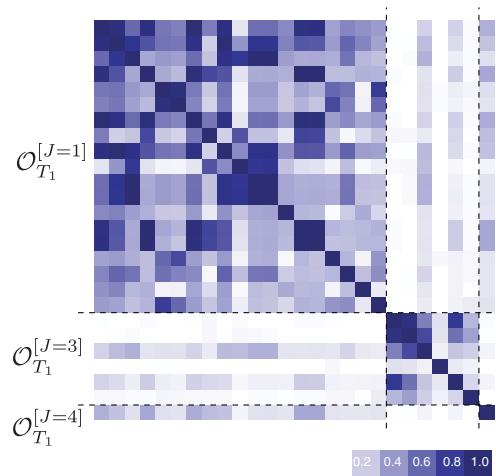

FIG. 2 (color online). Normalized correlation matrix $(C_{ij}/\sqrt{C_{ii}C_{jj}})$ on time slice 5 in the T_1^{--} irrep (*743*, 16^3). Operators are ordered such that those subduced from spin 1 appear first followed by spin 3 then spin 4.
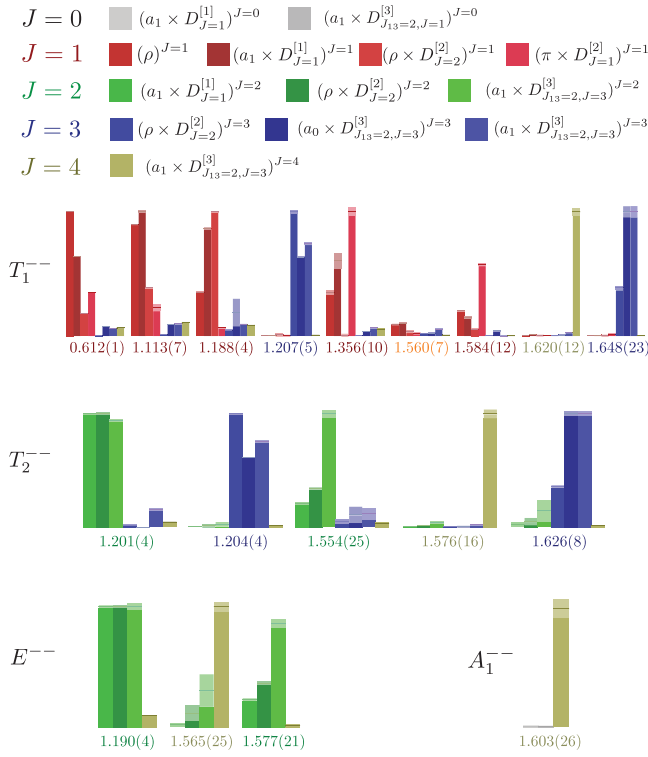
FIG. 3 (color online). Overlaps, Z, of a selection of operators onto states labeled by m/m_Ω in each lattice irrep, Λ^{--} (*743*, 16^3). Z's are normalized so that the largest value across all states is equal to 1. Lighter area at the head of each bar represents the one sigma statistical uncertainly.

operator $\mathcal{O}^{[J]}_\Lambda$ carries a "memory" of the continuum spin, J, from which it was subduced. If our lattice is reasonably close to restoring rotational symmetry, we would expect an operator subduced from spin J to overlap strongly only onto states of continuum spin J. In fact, this is clearly apparent even at the level of the correlator matrix as seen in

Fig. 2. Here the correlator matrix for T_1^{--} is observed to be approximately block diagonal when the operators are ordered according to the spin from which they were subduced. The elements outside the diagonal blocks are smallest when the operators feature zero, one, or two derivatives and are somewhat larger for three-derivative operators. Possible reasons for this will be discussed later in this section.

The effect is seen even more strongly at the level of individual states, where the "overlaps", $Z_i^{\mathfrak{n}} = \langle \mathfrak{n} | \mathcal{O}_i | 0 \rangle$ for a given state show a clear preference for overlap onto only operators of a single spin. In Fig. 3, we show the overlaps for a set of low-lying states in the Λ^{--} irreps of the *743* 16^3 calculation, the mass spectrum being shown in the second pane of Fig. 10. While we show only a subset of the operators for clarity, the same pattern is observed for the full operator set.

In fact, we can be more quantitative in our analysis and compare the overlaps obtained in different irreps. In the continuum, our operators are of definite spin such that $\langle 0 | \mathcal{O}^{J,M} | J', M' \rangle = Z^{[J]} \delta_{J,J'} \delta_{M,M'}$ and therefore $\langle 0 | \mathcal{O}^{[J]}_{\Lambda,\lambda} | J', M \rangle = \mathcal{S}^{J,M}_{\Lambda,\lambda} Z^{[J]} \delta_{J,J'}$ so that only the spin J states will contribute, and not any of the other spins present in the irrep Λ. Inserting a complete set of meson states between the operators in the correlator and using the fact that the subduction coefficients form an orthogonal matrix, $\sum_M \mathcal{S}^{J,M}_{\Lambda,\lambda} \mathcal{S}^{J,M*}_{\Lambda',\lambda'} = \delta_{\Lambda,\Lambda'} \delta_{\lambda,\lambda'}$, we obtain terms in the correlator spectral decomposition proportional to $Z^{[J]*} Z^{[J]}$; these terms do not depend upon which Λ we have subduced into, up to discretization uncertainties as described below. Hence, for example, a $J = 3$ meson created by a $[J = 3]$ operator will have the same Z value in each of the A_2, T_1, T_2 irreps. This suggests that we compare the independently obtained Z-values in each irrep. In Fig. 4 we show the extracted Z values for states suspected of being spin 2, 3, and 4 across the Λ^{--} irreps.
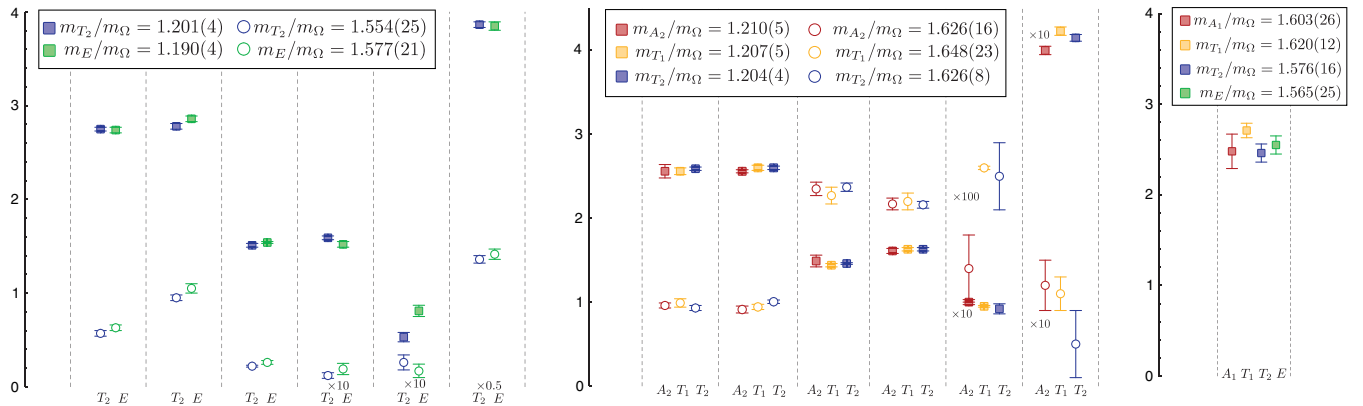

FIG. 4 (color online). A selection of Z values across irreps Λ^{--} for states suspected of being $J = 2, 3, 4$ (*743*, 16^3). Left to right, the operators are $(a_1 \times D^{[1]}_{J=1})^{J=2}$, $(\rho \times D^{[2]}_{J=2})^{J=2}$, $(\rho_2 \times D^{[2]}_{J=2})^{J=2}$, $(a_0 \times D^{[3]}_{J_{13}=2,J=2})^{J=2}$, $(b_0 \times D^{[3]}_{J_{13}=1,J=2})^{J=2}$, $(a_1 \times D^{[3]}_{J_{13}=0,J=1})^{J=2}$, $(\rho \times D^{[2]}_{J=2})^{J=3}$, $(\rho_2 \times D^{[2]}_{J=2})^{J=3}$, $(a_0 \times D^{[3]}_{J_{13}=2,J=3})^{J=3}$, $(a_1 \times D^{[3]}_{J_{13}=2,J=3})^{J=3}$, $(a_1 \times D^{[3]}_{J_{13}=2,J=2})^{J=3}$, $(b_1 \times D^{[3]}_{J_{13}=1,J=2})^{J=3}$, and $(a_1 \times D^{[3]}_{J_{13}=2,J=3})^{J=4}$.
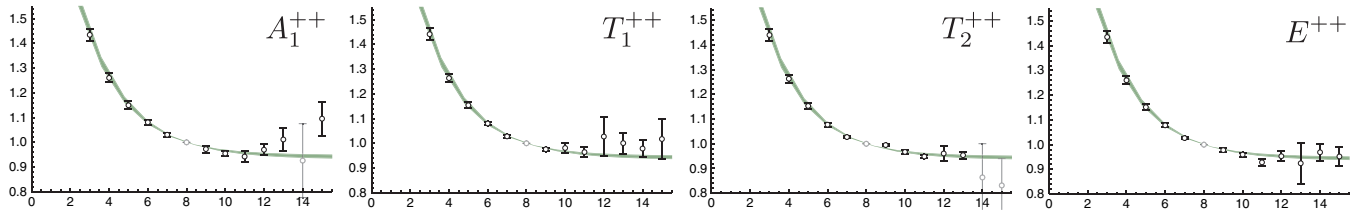
FIG. 5 (color online). Fit to the four subduced principal correlators of a 4^{++} meson using a common mass (*743*, 16^3). Plotted is $\lambda(t) \cdot e^{m(t-t_0)}$. Grey points not included in the fit.

As seen in Fig. 4, at finite lattice spacing there are deviations from exact equality. Some discretization effects scale with positive powers of the lattice spacing, such as the effect of using finite differences to represent derivatives. There are no dimension-five operators made of quark bilinears that respect the symmetries of lattice actions based on the Wilson formalism and that do not also transform trivially under the continuum group of spatial rotations. Thus, rotational symmetry breaking terms do not appear until $\mathcal{O}(a^2)$. This argument holds even though the action used in this work describes an anisotropic lattice. As a result, we expect the rotational breaking between lattice irreps to be suppressed in both the spectrum as well as for the wave-function overlaps. On the other hand, renormalization mixing of high mass-dimension operators with lower mass-dimension operators can give rise to effects scaling with negative powers of the lattice spacing and these we would expect to cause more trouble when Z values are to be used to determine spin. In practice, we do see the largest discrepancies for operators with three derivatives, but even here the effects are not so large as to prevent use of the method. We suggest that it is our use of smoothed fields[2] that has rendered these mixings relatively small, sensitive as they are to high-energy physics which has been filtered out.

In summary, we have demonstrated that the Z values of carefully constructed subduced operators can be used to identify the continuum spin of states extracted in explicit computation, as least on the lattices we have used.

Given that this is possible, suppose we confidently identify the components of a spin-J meson subduced across multiple irreps; what then should we quote as our best estimate of the mass of the state? The mass determined from fits to principal correlators in each irrep can differ slightly due to unavoidable discretization effects and avoidable fitting fluctuations (such as variations in fitting time-region). In practice, we have found that variations due to changes in the fitting of principal correlators are typically much larger than any discretization differences and we propose a simple scheme to minimize these in a final quoted mass. Rather than averaging the masses from independent fits to multiple principal correlators, we perform a

joint fit to the principal correlators with the mass being common. We allow a differing second exponential in each principal correlator so that the fit parameters are $m_\mathfrak{n}$, $\{m'^{\Lambda}_\mathfrak{n}\}$, and $\{A^{\Lambda}_\mathfrak{n}\}$. These fits are typically very successful with correlated χ^2/N_{dof} close to 1. An example for the case of 4^{++} components identified in A_1^{++}, T_1^{++}, T_2^{++}, E^{++} is shown in Fig. 5. When we present our final, spin-assigned, spectra, it is the results of such fits that we show.

VII. STABILITY OF SPECTRUM EXTRACTION

In this section, we consider to what extent the extracted spectrum changes as we vary details of the calculation, "keeping the physics constant". Variations to be considered are the specific reference time slice, t_0, used in the variational analysis, the set of meson operators used, and the number of distillation vectors. We will use the T_1^{--} irrep in the *743*, 16^3 dataset to demonstrate our findings.

A. Variational analysis and t_0

Our fitting methodology was described in Section V, where reconstruction of the correlator was used to guide us to an appropriate value of t_0. As seen in Fig. 6, for $t_0 \gtrsim 6$, the low-lying mass spectrum is rather stable under variations of t_0. This appears to be mostly due to the inclusion of a second exponential term in Eq. (4), which is able to absorb much of the effect of other states "leaking" into this principal correlator through use of an inaccurate orthogonality. The contribution of this second exponential typically falls rapidly with increasing t_0 both by having a smaller A and a larger m'.

Overlaps, $Z^i_\mathfrak{n} = \langle \mathfrak{n} | \mathcal{O}_i | 0 \rangle$, can show more of a sensitivity to t_0 values being too low as one might expect given the argument of an incorrect orthogonality in the generalized eigenvector space at small t_0. In Fig. 7, we present overlaps of various $J = 1$ states onto an operator subduced from $J = 1$ and the overlap of an extracted $J = 4$ state onto the only $J^{PC} = 4^{--}$ operator in our basis. Clearly, in the $J = 4$ case, one only extracts a stable Z for large t_0, which is likely due to heavier $J = 4$ states only here becoming negligible contributions to $C(t_0)$.

We note that one may fit the extracted $Z(t_0)$ with either a constant or a constant plus an exponential as shown in Fig. 7. Since the data between t_0 values are strongly correlated, the statistical uncertainty is not significantly

_____

[2]All gauge links are stout-smeared and the distilled quark fields are effectively low-momentum filtered.
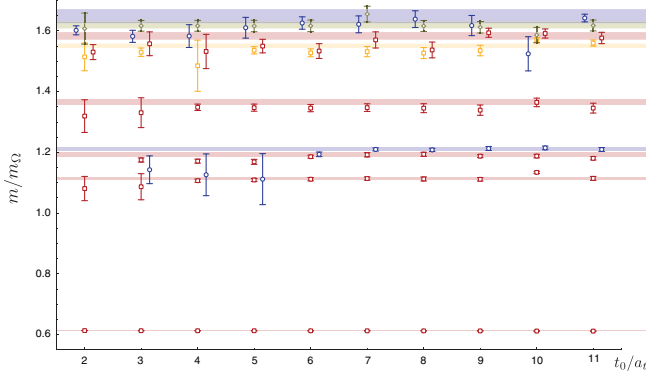
FIG. 6 (color online).   Extracted T_1^{--} mass spectrum as a function of t_0. Horizontal bands to guide the eye.

decreased by this procedure, but it does seem to "average out" some of the fluctuations in fitting at each t_0.

In summary, it appears that variational fitting is reliable provided t_0 is "large enough". Using two-exponential fits in principal correlators, we observe relatively small t_0 dependence of masses, but more significant dependence for the Z values which we require for spin-identification.
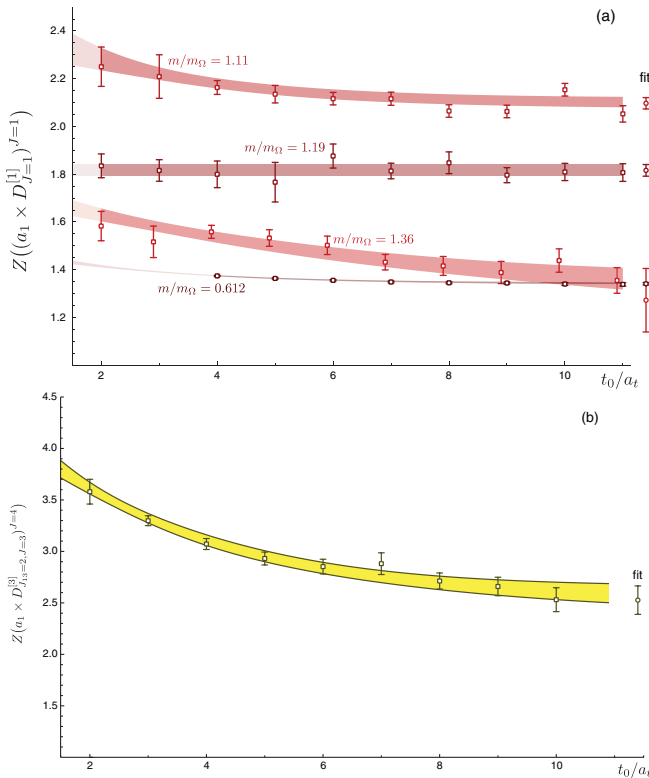
FIG. 7 (color online).   Extracted overlaps as a function of t_0. Fits to a constant or to a constant plus a decaying exponential shown by the colored regions. (a) $J^{PC} = 1^{--}$ overlaps onto $(a_1 \times D_{J=1}^{[1]})^{J=1}$.   (b) $J^{PC} = 4^{--}$ overlap   onto $(a_1 \times D_{J_{13}=2,J=3}^{[3]})^{J=4}$.

B. Changing the operator basis

Our approach, as described in Section IV, is to construct a variational correlator matrix featuring all operators available to us in a given irrep at up to three derivatives. Here we consider the effect on the extracted spectrum of reducing the size of this operator basis. In the plots that follow, we will use the color-coding described in Table V to indicate spin-assignments.

In the first four columns of Fig. 8, the operator basis is reduced by discarding operators, first discarding those whose diagonal correlators are noisiest and then, in Fig. 8 [column (d)], discarding all three-derivative operators except the one $J = 4$ operator. We observe that it is only high in the spectrum that any change takes place and that there it is only at the level of statistical fluctuations. In Fig. 8 (d), the first excited $J = 3$ state is no longer extracted—this is most likely due to the basis only retaining two $J = 3$ operators.

In the next four columns, we deliberately discard operators we believe are important. In Fig. 8 [column (e)], all operators featuring commutators of derivatives are discarded. As discussed later in this manuscript, these operators may have good overlap onto states containing an excited gluonic field. The state at $m/m_\Omega \sim 1.35$ is observed, using the full basis of operators, to have large overlap onto a commutator operator, $(\pi \times D_{J=1}^{[2]})^{J=1}$ along with smaller overlaps onto noncommutator operators such as ρ. In column Fig. 8 (e), the commutator operators being discarded, we find that this state is less cleanly extracted when it can only be produced through its suppressed noncommutator overlaps. Otherwise the spectrum in Fig. 8 (e) is rather similar to that obtained with the full operator basis.

In Fig. 8 [column (f)], all operators subduced from spin $J = 3$ are discarded. The observed spectrum is almost identical to that with the full basis with the expected exception of the previously identified $J = 3$ states. This would appear to suggest that one cannot rely upon discretization corrections to continuum $J = 1$ operators to reliably produce $J = 3$ states. In Fig. 8 [column (g)], the continuum $J = 4$ operator is also discarded and the $J = 4$ state vanishes. Finally, in Fig. 8 [column (h)], the full operator basis, less the continuum $J = 4$ operator is used yielding a spectrum that lacks only the $J = 4$ state.

TABLE V.   Color-coding used in spectrum irrep plots.

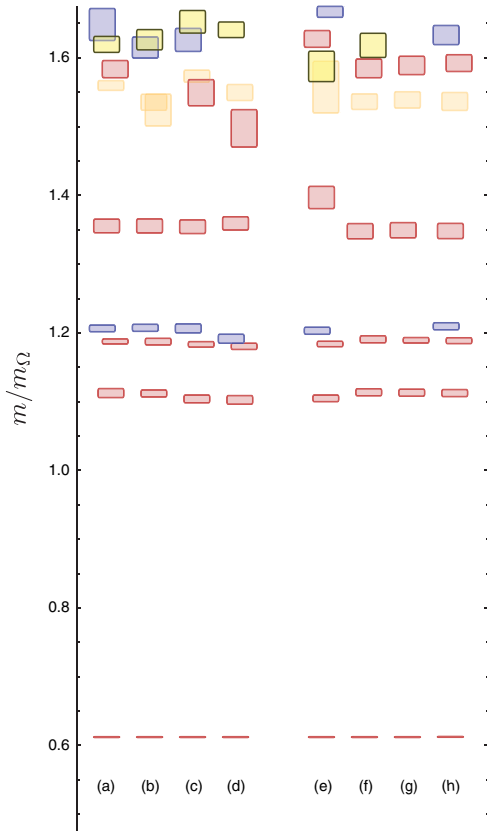| black	$J = 0$
red	$J = 1$
green	$J = 2$
blue	$J = 3$
yellow	$J = 4$
orange	undetermined J
grey	badly determined mass

FIG. 8 (color online).   Extracted T_1^{--} mass spectrum for various operator bases. (a)–(d) are "reasonable" operator bases, (e)–(h) discard important operators. (a) Full basis (dim= 26), (b) Full basis less two noisiest $\mathcal{O}^{J=1}$ and noisiest $\mathcal{O}^{J=3}$ (dim= 23), (c) Full less four noisiest $\mathcal{O}^{J=1}$ and two noisiest $\mathcal{O}^{J=3}$ (dim= 20), (d) No three-derivative operators except $\mathcal{O}^{J=4}$ (dim= 13), (e) No operators with commutators of derivatives (dim= 15), (f) No $\mathcal{O}^{J=3}$ (dim= 20), (g) No $\mathcal{O}^{J=3,4}$ (dim= 19), (h) No $\mathcal{O}^{J=4}$ (dim= 25).

In summary, one should be sure to have operators with continuum overlap on to all the spins you expect to see. There is apparently little benefit, in terms of improving the precision of determination of the low-lying spectrum, of reducing the operator basis size by discarding operators.

C. Number of distillation vectors

The results presented so far came from analysis of correlators computed on 16^3 lattices using 64 distillation vectors. We might wonder how the determination of the spectrum varies if one reduces the number of distillation vectors and thus reduces the computational cost of the calculation. This is particularly important given that, as shown in [20], to get the same smearing operator on larger volumes one must scale up the number of distillation vectors by a factor equal to the ratio of spatial volumes. To scale up to a 32^3 lattice this would require $64 \times \left(\frac{32}{16}\right)^3 = 512$ vectors, which is not currently a realizable number without using stochastic estimation [38].

In Fig. 9 we show the low-lying part of the extracted T_1^{--} spectrum on the 743 16^3 lattice as a function of the number of distillation vectors used in the correlator construction. It is clear that the spectrum is reasonably stable for $N \gtrsim 32$ but that the spectrum quality degrades rapidly for fewer vectors.

It is also possible within distillation to implement a smearing operator other than $\Box = \sum_{n=1}^{N} \xi_n \xi_n^\dagger$. This is particularly relevant for large N, where this smearing choice tends toward the identity and hence does not actually filter out high-energy modes. An alternative smearing includes a weight function as $\Box_w = \sum_{n=1}^{N} w(\lambda_n) \xi_n \xi_n^\dagger$, where $w(\lambda_n)$ might, for example, be a Gaussian damping $e^{-\sigma^2 \lambda_n / 4}$. In Fig. 9, we also show the spectrum obtained using $N = 64$ and $\sigma = 5.7$ which, as shown in the inset, is a smearing radius that crudely approximates using only 24 distillation vectors. The thus extracted spectrum differs very little from the $N = 64$ spectrum, suggesting that with 64 vectors we are still far away from the "unsmeared" limit.

One place (not shown in Fig. 9) where the effect of reduction of the number of distillation vectors is seen clearly is for high-spin states. In particular the 4^{--} state seen at $m/m_\Omega \sim 1.6$ in T_1^{--} is not reliably extracted for $N < 48$. The need to have large numbers of distillation vectors to reliably extract high-spin mesons can be described in a simple free-field picture: In the continuum without gauge-fields, the eigenvectors of the Laplacian $(-\nabla^2 \xi = k^2 \xi)$ can be expressed as $\xi(\vec{r}) = e^{i\vec{k}\cdot\vec{r}} = 4\pi \sum_\ell i^\ell j_\ell(kr) \sum_m Y_\ell^{m*}(\theta, \phi) Y_\ell^m(\hat{k})$. From this expression, it would appear that all ℓ values should contribute for any value of the eigenvalue k^2 and that high-spin states should be excited even by low eigenvectors. But this argument does not take account of the radial behavior which must be compared to the typical size of hadrons. The spherical Bessel function $j_\ell(kr)$ is peaked at low values of kr with the peak position moving out to larger kr for
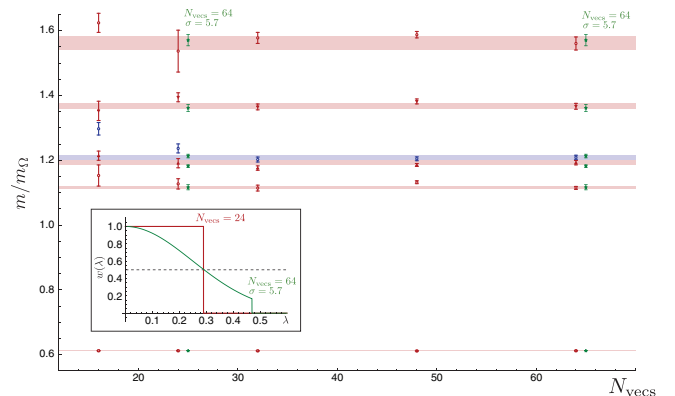

FIG. 9 (color online).   Extracted T_1^{--} mass spectrum as a function of number of distillation vectors. Green points and inset show the effect of using a modified smearing operator $\Box_w = \sum_{n=1}^{N} w(\lambda_n) \xi^n \xi^{n\dagger}$ with $w(\lambda_n) = e^{-\sigma^2 \lambda_n / 4}$.

larger ℓ. Thus, since hadrons are only of finite size, R, in order that the peak of $j_\ell(kr)$ remain within $r < R$ as ℓ increases, one must also increase the value of k. Thus, to have considerable amplitude multiplying Y_ℓ and hence large overlap onto high-spin mesons, as ℓ increases one must include eigenvectors of higher eigenvalue, k.[3]

In summary, one is limited as to how few distillation vectors can be used if one requires reliable extraction of high-spin states. The results shown here suggest 48 distillation vectors on a 16^3 lattice is the minimum, so 96 distillation vectors on a 20^3 lattice are likely to be required.

VIII. RESULTS

As outlined in Section II, our first results are obtained on lattices with pion masses between 400 and 700 MeV. The heaviest pion mass corresponds to the three-flavor symmetric point, while the lower masses have lower light-quark masses but the same bare strange quark mass; these are found to have only mild $SU(3)_F$ breaking, as indicated by m_K / m_π which reaches only 1.4 on the lightest lattice, well below the physical value of 3.5. For each lattice (except one), we compute correlators on two volumes, $16^3 \times 128$ and $20^3 \times 128$. More complete details of the number of configurations, time sources and distillation vectors used are given in Table I.

A. $m_\pi \sim 700$ MeV results (*743*)

This is an example of an exact $SU(3)$-flavor symmetric calculation. Since we are computing only the connected two-point correlators, we will obtain the mass spectrum of degenerate octets (e.g., degenerate pions, kaons and η_8). Results on 16^3 lattices have already been reported in Ref. [8]. To obtain singlet states like the η_1, which with exact flavor symmetry cannot mix with the η_8, we would need disconnected two-point correlators.

Variational analysis as described in previous sections leads to the irrep spectra from 16^3 lattices shown in Fig. 10. The color-coding, tabulated in Table V, indicates the continuum spin as determined by methods described in Section VI. The Λ^{--} overlaps are shown in Figs. 3 and 4. If the spin of a state is not unambiguously determined by the methods of Section VI, it is represented by an orange box. On the other hand, if a state is extracted in the variational analysis but its mass cannot be accurately determined from fits to the principal correlator, it is represented by a grey box.

In Fig. 11, we show side-by-side the spectra obtained from 16^3 and 20^3 lattices. We note that there is really no change significantly outside statistical fluctuations between the two volumes. We also note in passing that the 128 distillation vectors used on the 20^3 lattices give a

---

[3]This analysis is somewhat oversimplified since in fact the size of hadrons is likely to increase with increasing spin.
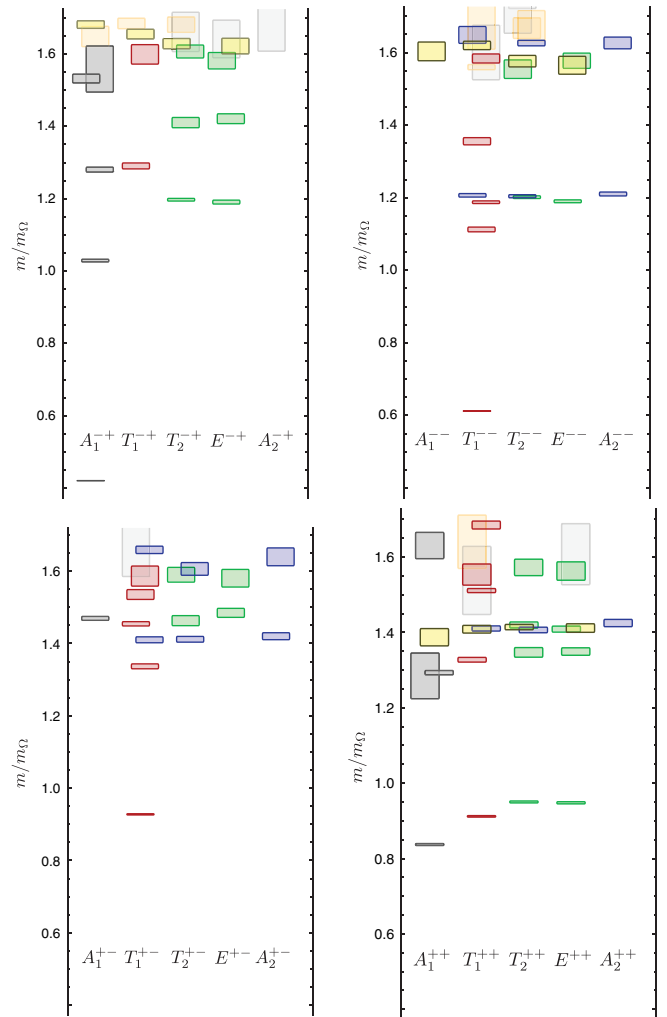

FIG. 10 (color online). Extracted spectra by irrep from *743* 16^3 lattices.

smearing that is essentially equivalent to that obtained by using 64 distillation vectors on the 16^3 lattices. In fact, we observe that the independently extracted Z values between the two volumes scale rather accurately as $\sqrt{\frac{16^3}{20^3}}$.

Given the success of spin-identification we can summarize the results in a spectrum labeled by continuum J^{PC} quantum numbers, Fig. 12. Here we show only well-determined low-lying states.

There are a number of notable features within this spectrum. We will argue later that the pattern of states and the lack of volume dependence appears to be incompatible with the presence of discrete meson-meson energy levels and as such we are lead to interpret the spectrum in terms of single-hadron states. Under that assumption, there appears to be much of the $n^{2S+1}L_J$ distribution of non-exotic states predicted by the $q\bar{q}$ quark model (e.g., [39]). The left-hand pane of Fig. 12 has candidates for a ground-state S-wave pair $(0^{-+}, 1^{--})$ and a radial excitation at around $m/m_\Omega \sim 1.1$. There is a complete $(1, 2, 3)^{--}$,
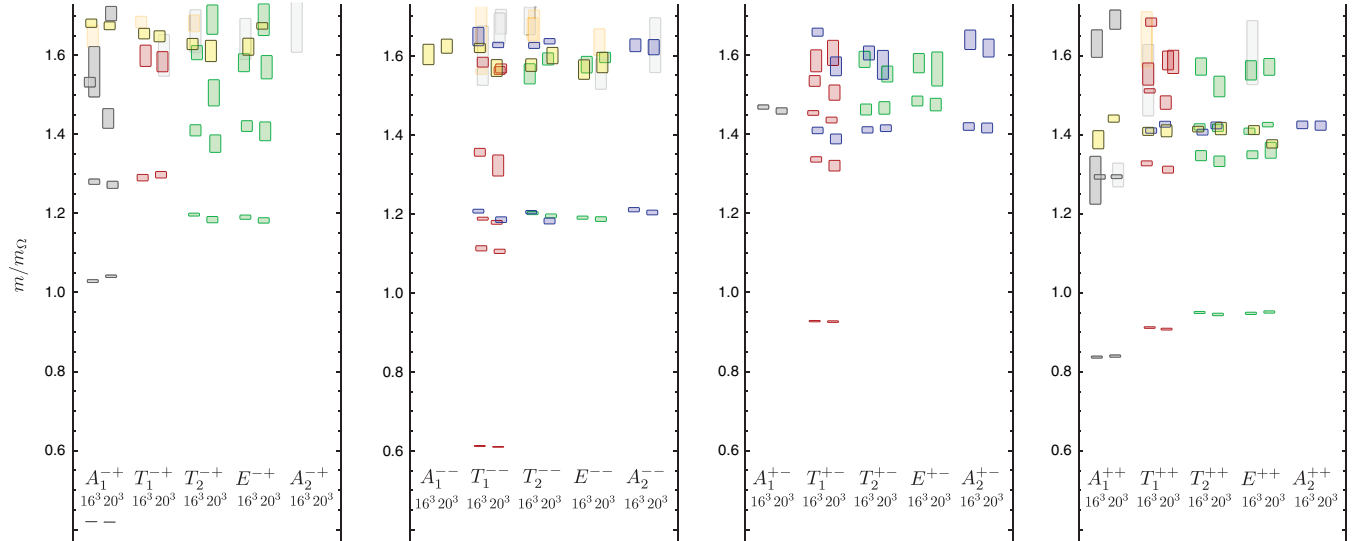
FIG. 11 (color online).   Extracted spectra by irrep from *743* 16^3 and 20^3 lattices.

2^{-+} *D*-wave set around $m/m_\Omega \sim 1.2$. The region around $m/m_\Omega \sim 1.6$ appears to contain parts of a *D*-wave radial excitation and a *G*-wave $((3, 4, 5)^{--}, 4^{-+})$.[4] In the middle pane of Fig. 12, there is a clear *P*-wave, $((0, 1, 2)^{++}, 1^{+-})$ around $m/m_\Omega \sim 0.9$ and a probable radial excitation near $m/m_\Omega \sim 1.3$. At $m/m_\Omega \sim 1.4$, there is a complete *F*-wave, $(2, 3, 4)^{++}, 3^{+-}$.

In the right-hand pane of Fig. 12, we see clearly a set of exotic J^{PC} states, not accessible to a simple $q\bar{q}$ pair. Such states can be described in terms of constituents if additional degrees-of-freedom, either gluonic or extra $q\bar{q}$ pairs are included. If the extra component is gluonic, the states are known as hybrid mesons and within models of gluonic excitation, such as the flux-tube model [40], there is usually a roughly degenerate set of 1^{-+}, 0^{+-}, and 2^{+-} states. A hybrid nature for these states is suggested by the large overlap onto operators with essential nontrivial gluonic structure as described below. In this calculation, we observe a 1^{-+} lightest, with a pair of 0^{+-} and 2^{+-} states nearly degenerate a little higher in mass. A second 2^{+-} is then close to a second 1^{-+}. States with exotic 0^{--} and 3^{-+} quantum numbers are found to be considerably heavier, well above $m/m_\Omega = 1.6$.

There are also a number of *nonexotic* quantum numbered states which do not appear to fit into the $q\bar{q}$ $n^{2S+1}L_J$ classification. The 0^{-+}, 1^{--} pair at $m/m_\Omega \sim 1.3$ is probably too light to be the second radial excitation of the *S*-wave (most likely the pair near $m/m_\Omega \sim 1.55$) and is partnered with a totally unexpected 2^{-+} state. There may be excess states too in the positive parity sector, but the situation is not totally clear above $m/m_\Omega \sim 1.4$. We note that the mass scale of these first excess states is comparable

to that of the lowest-lying exotic states shown in the right-hand pane of Fig. 12. Furthermore, these states have characteristically different overlap behavior compared to most other extracted states: they all overlap considerably onto operators featuring the commutator of two derivatives, that is the gluonic field-strength tensor.

Given the large overlap onto operators requiring a nontrivial gluonic field distribution, we identify these states as hybrid mesons with nonexotic quantum numbers. Such nonexotic hybrids are predicted in models that assume nontrivial gluonic field configurations like the flux-tube model or constituent gluon models. In principle, such states can mix strongly with regular quark-model $q\bar{q}$ states leaving a spectrum which is not simple to interpret. In our results such large mixing may be present for the "excess" 0^{-+} state which has a large overlap also onto operators like $\bar{\psi}\gamma_5\psi$; however, this mixing does not appear to be present to the same degree for the 1^{--} state.

Detailed model-dependent interpretation of the spectrum, comparing the overlap values with the expectations of a bound-state quark model (analogous to that done for charmonium in [41]) and considering the degree of mixing of nonexotic hybrids and quark-model states will follow in a subsequent publication.

B. Quark-mass dependence

Here we move away from the $SU(3)$ flavor point by lowering the mass of two degenerate "light" flavors and keeping one remaining strange flavor heavy. We have access to isovector mesons from the connected correlators with a light quark and a light antiquark, and kaons from the connected correlators with a light quark and a strange antiquark. It is also possible for us to compute the connected part of correlators with both quark and antiquark being strange, the so-called strangeonium. We recognize
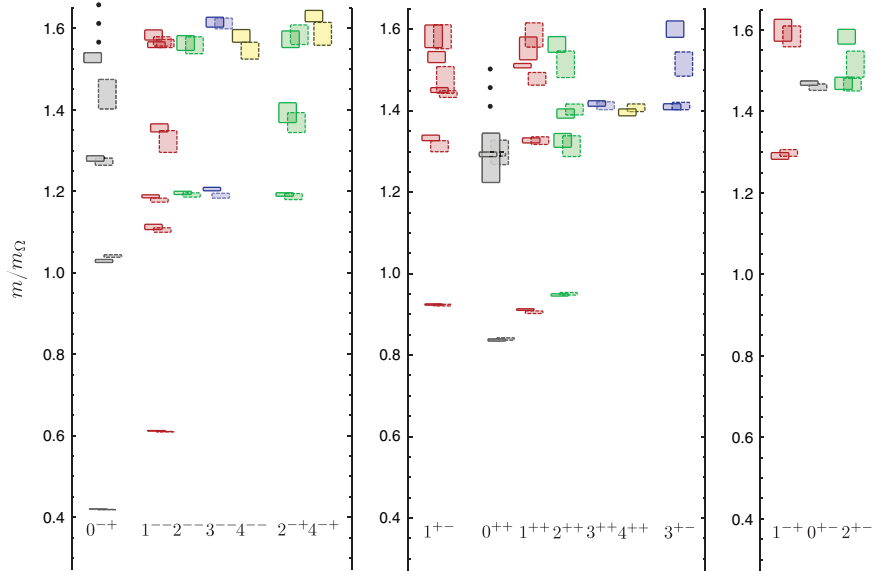
---

[4]We have no operators capable of producing a spin-5 meson in the continuum.

FIG. 12 (color online).   Spin-identified spectrum of isovector (octet) mesons from the *743* lattices. 16^3 (solid) and 20^3 (dashed) spectra agree well. Ellipses indicate that there are heavier states with a given J^{PC} but that they are not well determined in this calculation.

that neglecting the disconnected contributions to these diagrams leads to a nonunitary description of this particular element of our calculation. Of course it is also true that strangeonium states are not necessarily QCD eigenstates since being isoscalars they can mix with light-light isoscalars and pure-glue states through disconnected diagrams.[5] The classic extreme examples are the η, η' system which is mixed almost as $SU(3)_F$ octet-singlet and the ω, ϕ system which is mixed almost as $\ell\bar{\ell}$, $s\bar{s}$.

In the figures, we show extracted state masses as a function of $\ell_\Omega \equiv \frac{9}{4}\frac{(a_t m_\pi)^2}{(a_t m_\Omega)^2}$ which we use as a proxy for the quark mass [29]. The state masses are presented via $\frac{a_t m_H}{a_t m_\Omega} m_\Omega^{\text{phys}}$. The ratio of the state mass (m_H) to the Ω-baryon mass computed on the same lattice removes the explicit scale dependence and multiplying by the physical Ω-baryon mass conveniently expresses the result in MeV units. This is clearly not a unique scale-setting prescription, but it serves to display the data in a relatively straightforward way. We remind the reader that the data between different volumes and quark masses are uncorrelated since they follow from computations on independently generated dynamical gauge-fields.

1. Isovector mesons

Figures. 13–17 show the extracted spin-assigned spectra for mesons of isospin-1 having a range of J^{PC} quantum

numbers (the neutral members of the $I = 1$ triplet are eigenstates of C, the charged members are eigenstates of G-parity with $G = -C$). We use the Particle Data Group (PDG) [42] nomenclature for meson states throughout. In those cases where two states are almost degenerate, we shift one in the horizontal direction by an amount $\delta\ell_\Omega = 0.005$ for clarity. In some cases, for comparison, we plot the mass of the lightest meson-meson pair which in S-wave would have the appropriate quantum numbers—the mass follows from the simple sum of the extracted masses on these lattices. This may involve a so far undetermined isoscalar mass and in these cases we use the approximations $m_\omega \approx m_\rho$, $m_{f_2} \approx m_{a_2}$ and the crudely estimated η mass from [29]. Occasionally, we extract a low-lying state that is reasonably robust against the changes in analysis detailed in Section VII, but whose principal correlator is quite noisy leading to a relatively poorly determined mass—we show these states with dashed symbols.

Not shown are results for 0^{--} isovectors, the ρ_0, which are exotic. The lightest such state we extract is at least 2 GeV heavier than the ρ at all our quark masses. The exotic 3^{-+}, the π_3, is found to be similarly heavy.

2. Kaons

In the kaon sector, we no longer have charge-conjugation as a good quantum number, with only J^P remaining in the continuum which is then subduced into Λ^P on a cubic lattice. We compute a correlator matrix for a given Λ^P using the concatenated list of all Λ^{P+} and Λ^{P-} operators.

Using a combination of experiment and models [43,44], there are suggestions that resonant kaon states are mixtures

---

[5]Work is ongoing within the Hadron Spectrum Collaboration [20] to utilize distillation methods to efficiently compute disconnected two-point functions, allowing extraction of the true QCD eigenstates.
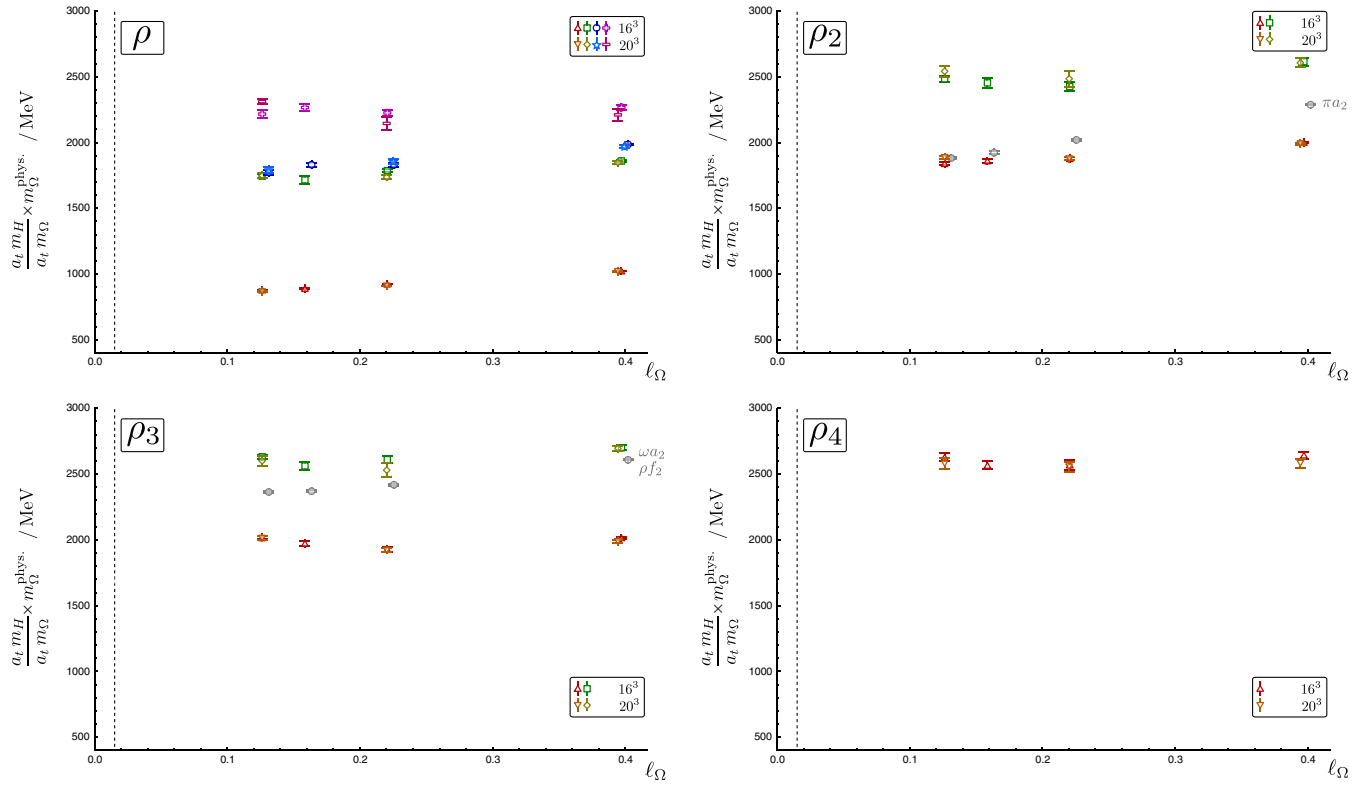
FIG. 13 (color online). Lightest isovector states, ρ_J; neutral members with quantum numbers J^{--}.
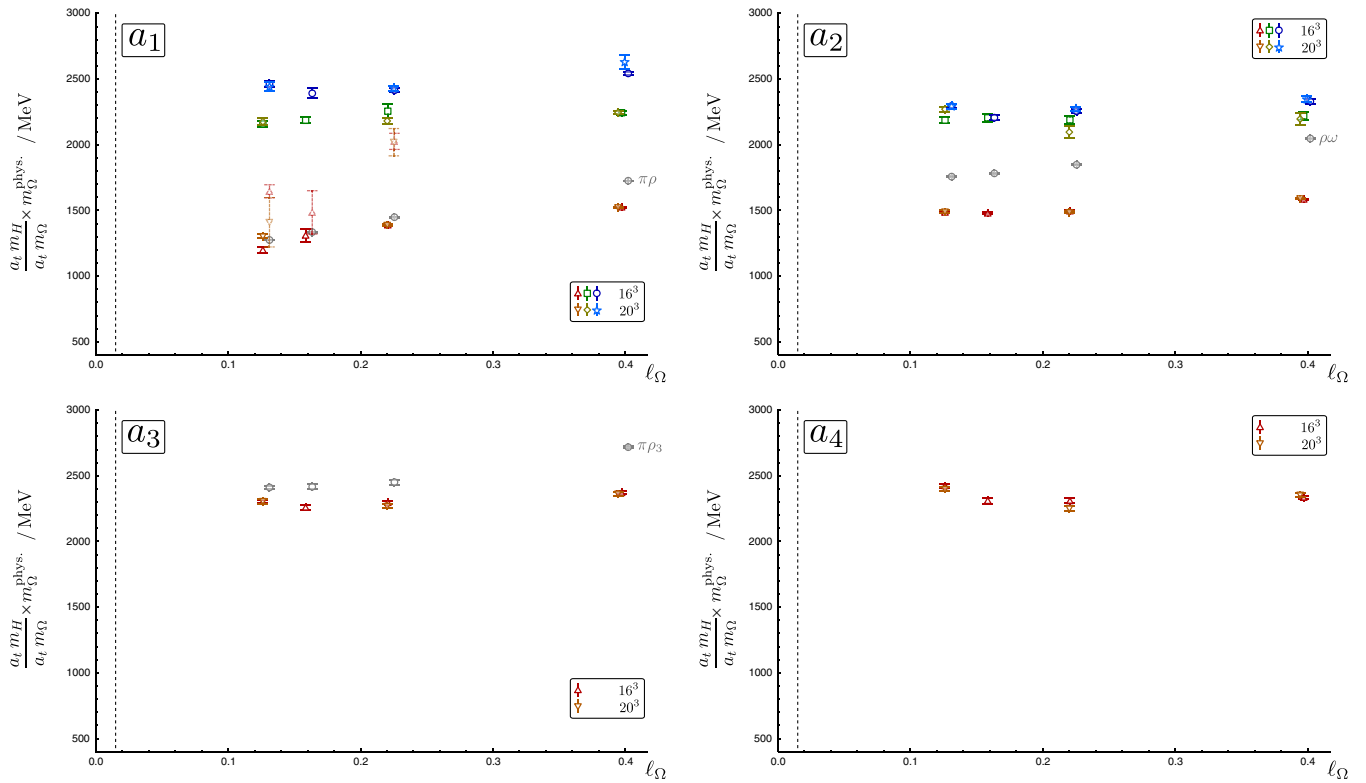

FIG. 14 (color online). Lightest isovector states, a_J; neutral members with quantum numbers J^{++} (the a_0 states are shown in Fig. 16).
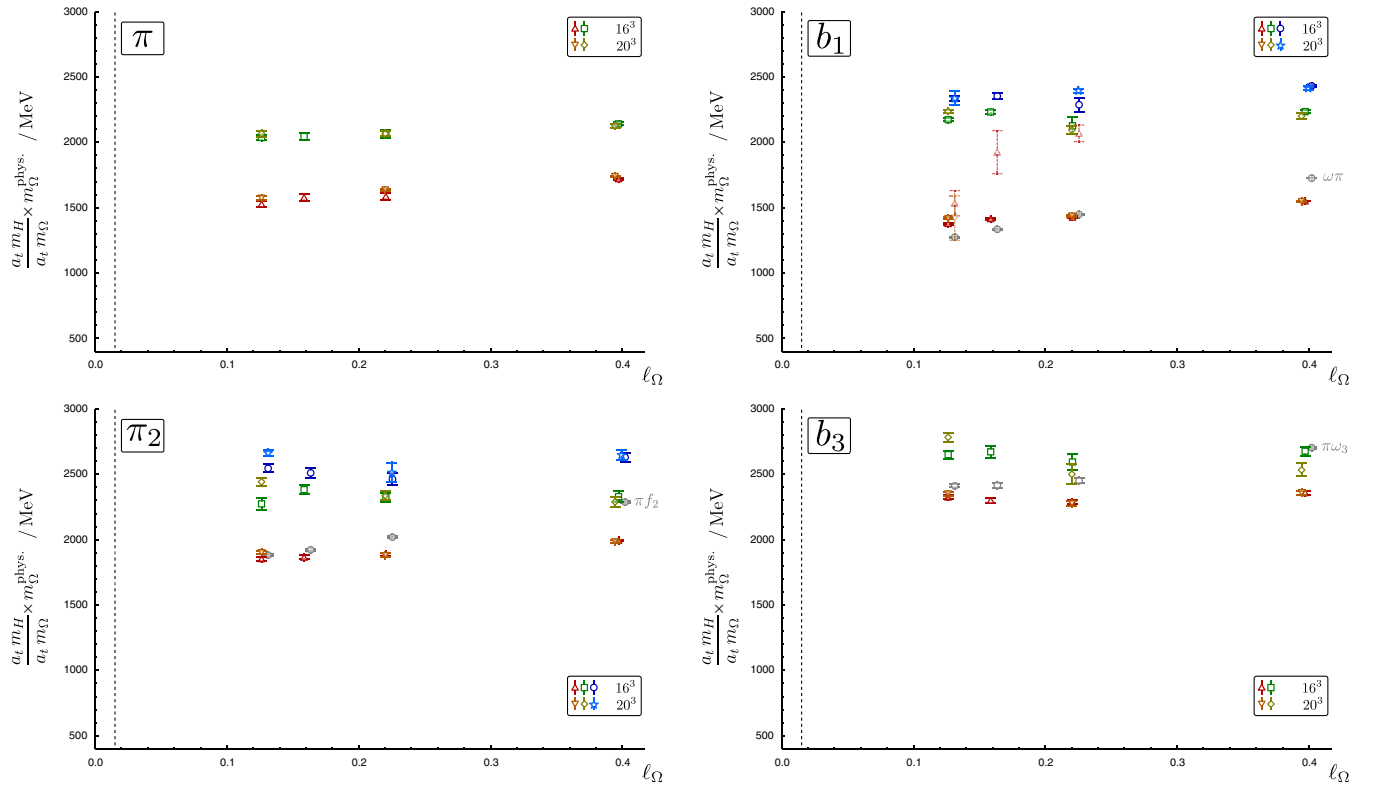
FIG. 15 (color online).   Lightest nonexotic isovector states, $\pi_J(J^{-+})$ and $b_J(J^{+-})$; the ground-state π is not shown.
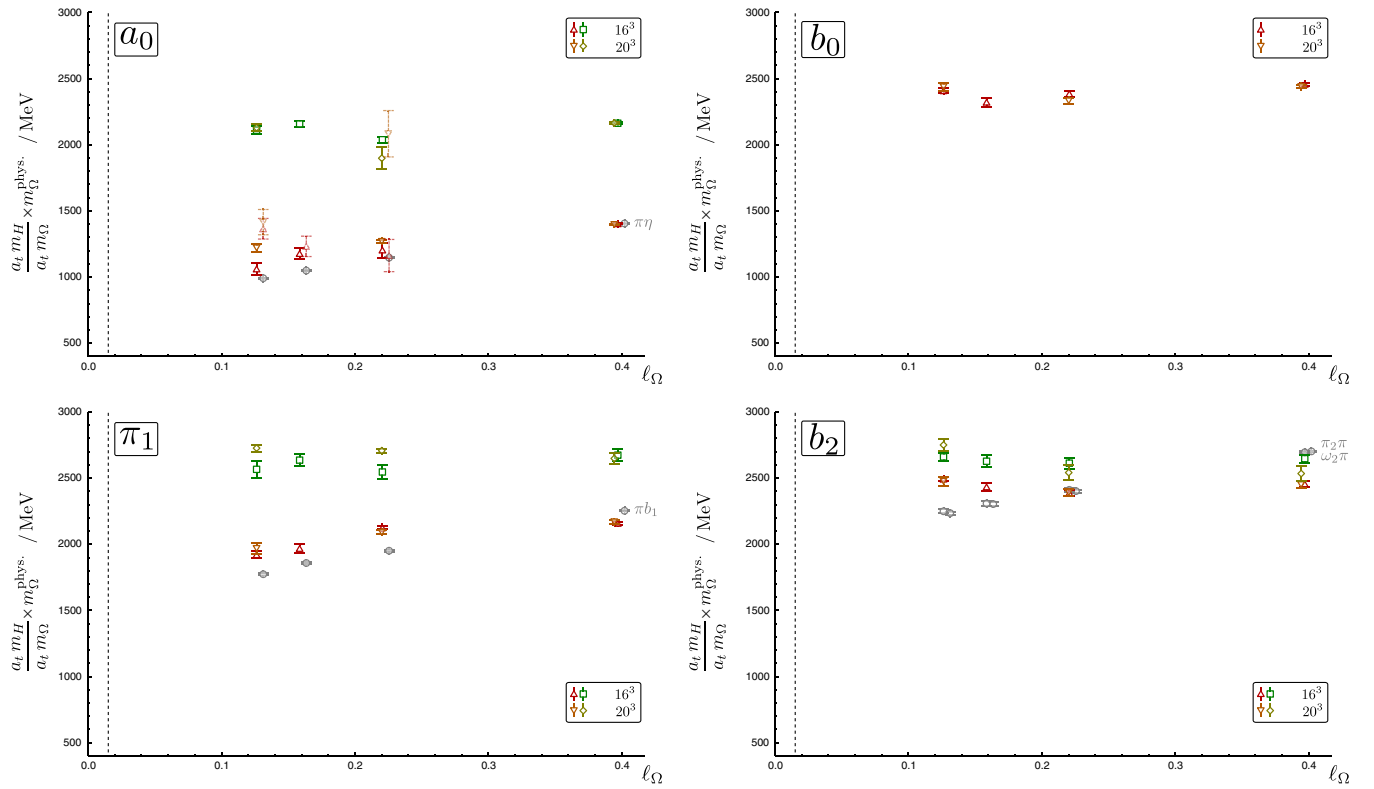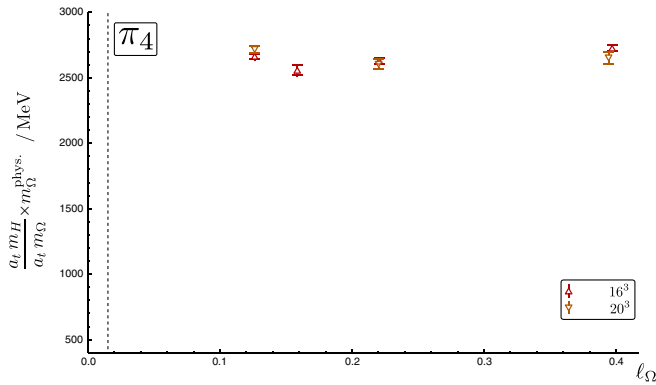

FIG. 16 (color online).   Lightest isovector states: scalar and exotics, $a_0(0^{++})$, $\pi_1(1^{-+})$, $b_J(J^{+-})$.

FIG. 17 (color online). $\pi_4(4^{-+})$.

of basis states of opposite C with a rather large mixing angle. For example, the axial kaons, $K_1(1270)$, $K_1(1400)$, are suggested to be mixtures of basis states $K_{1A}(C = +)$, $K_{1B}(C = -)$ with a mixing angle near 45°. Clearly this mixing relies upon being far away ($m_K^{\mathrm{phys}}/m_\pi^{\mathrm{phys}} = 3.5$) from the $SU(3)_F$ limit, since in that limit there is effectively restoration of (a generalization of) C-symmetry. All the lattices presented in this paper can be considered to be rather close to the $SU(3)_F$ limit ($1 \leq m_K/m_\pi \leq 1.39$) and we observe little or no mixing. This is suggested at the correlator level (see Fig. 18 for the 840 16^3 correlator), and verified in the Z values of the spectrum extraction [see Fig. 19 for the 808 16^3 lattice (left) and the 840 16^3 lattice (right)]. While the 840 lattice shows a greater degree of opposite C mixing than the 808, indicating an increased breaking of $SU(3)_F$ symmetry, the mixing is still very small in absolute terms and states are approximate eigenstates of C. The 840 kaon spectrum is shown in Fig. 20 with the dominant C-eigenstate noted for each state.

The light-quark-mass dependence of kaon states is displayed in Figs. 21–23, where color-coding indicates the dominance of C-eigenstates within the spectrum.
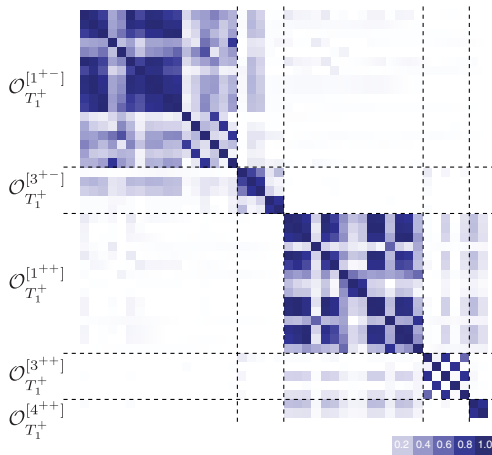
FIG. 18 (color online). Normalized correlation matrix $(C_{ij}/\sqrt{C_{ii}C_{jj}})$ on time slice 5 in the T_1^+ kaon irrep on 840 16^3 lattice. Operators with $C = -$ first, $C = +$ second.
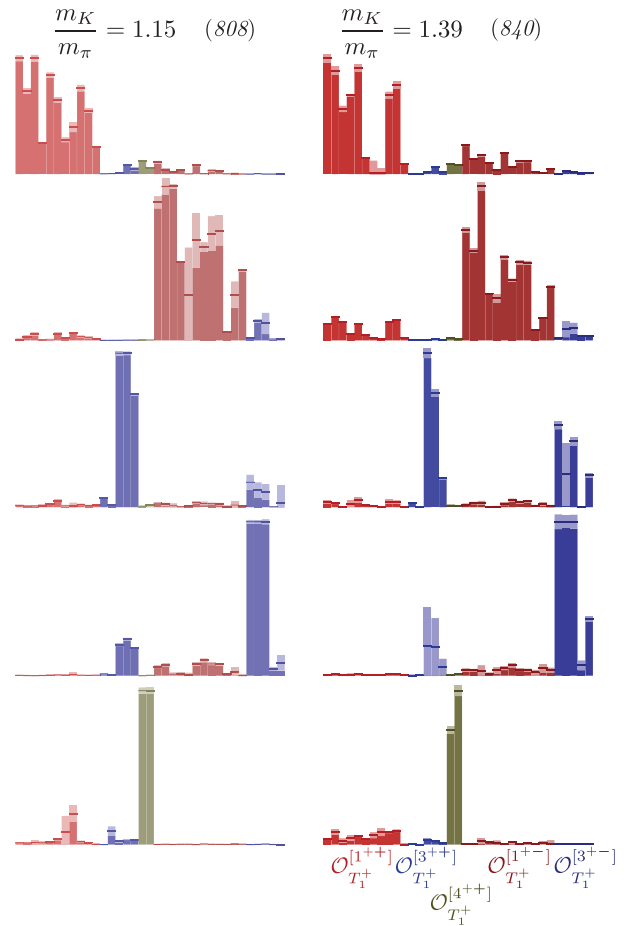
FIG. 19 (color online).   Overlaps, Z, of T_1^+ kaon operators onto lightest two $J = 1$, lightest two $J = 3$ and lightest $J = 4$ states for 808 16^3 (left) and 840 16^3 (right) lattices. Operators with $C = \pm$ are grouped to show clear separation. Normalization as in Fig. 3.
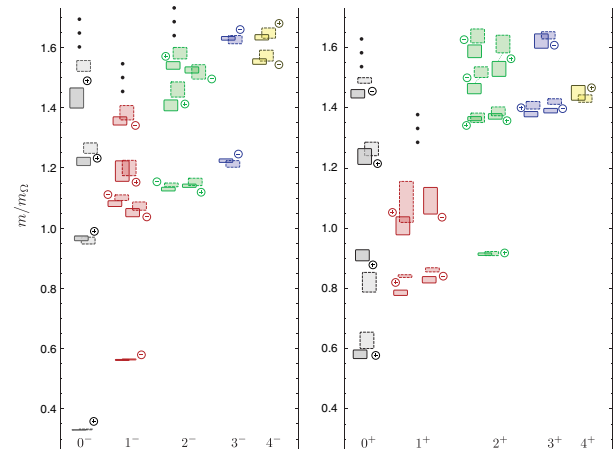
FIG. 20 (color online).   Spin-identified spectrum of kaons from the 840 lattices. 16^3 (solid lines) and 20^3 (dashed lines) spectra mostly agree well. The plus and minus symbols indicate the dominance of a $C = \pm$ eigenstate in that state. Ellipses indicate that there are heavier states with a given J^{PC} but that they are not well determined in this calculation. The rather dense spectrum of axial kaons above $m/m_\Omega \sim 1.3$ is suppressed for clarity.
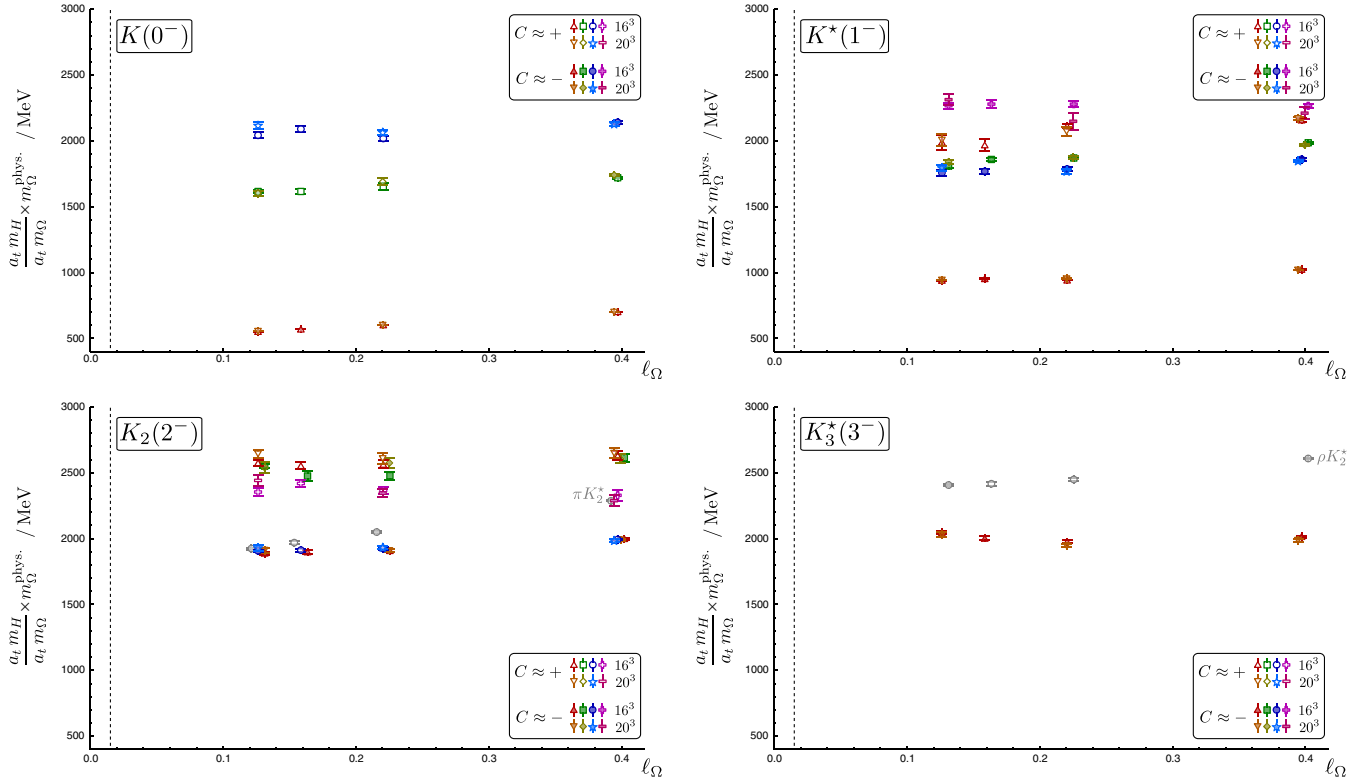
FIG. 21 (color online).   Lightest negative parity kaons. Hollow (filled) symbols indicate dominance of $C = +(-)$.

3. Strangeonium

In Fig. 24, we show only a subset of possible strangeonium J^{PC}, those for which there is some phenomenological evidence that the QCD eigenstates are in fact close to being pure $s\bar{s}$. We note that using this particular scale-setting scheme we observe light-quark-mass dependencies that are very flat.

IX. MULTIMESON STATES

In the previous section, we presented the extracted spectra from calculations with four different light-quark masses on two different lattice volumes. In each case, we were able, using the operator overlaps, to match states across irreps that we believe are subduced from the same continuum spin state. This suggests an interpretation of the spectrum in terms of single-hadron states, while in principle our correlators should receive contributions from all eigenstates of finite-volume QCD having the appropriate quantum numbers. This includes multimeson states which in finite volume have a discrete spectrum. In fact, in a theory of noninteracting mesons, the spectrum is rather simple, being approximately[6]

$$m[A(\vec{p})B(-\vec{p})] = \sqrt{m_A^2 + |\vec{p}|^2} + \sqrt{m_B^2 + |\vec{p}|^2}, \quad (5)$$

where only discrete values of the momentum $\vec{p}$ are allowed by the boundary conditions: $a_s\vec{p} = \frac{2\pi}{L_s}(n_x, n_y, n_z)$ (L_s is the spatial lattice extent in lattice units, i.e., 16 or 20 for the lattices we are using). Clearly this spectrum, with the exception of the states with $\vec{p} = (0, 0, 0)$, will change considerably under changes in volume. In essence, the distribution of single-particle states across irreps is determined by discretization effects from the finite lattice spacing which we find to be small. On the other hand, the distribution of meson-meson states is determined by the cubic symmetry of the lattice box boundary, and we would only expect the distribution to resemble that of full rotational symmetry in the limit of small $\frac{2\pi}{L_s a_s}$ compared to the splitting between hadrons. We are not close to this limit on these lattices where the minimum momentum unit is $\gtrsim$ 500 MeV.

Within QCD, mesons interact and this interaction has a range of possible forms, for example: the repulsive interaction of two pions in the isospin 2 channel, the somewhat attractive interaction of two pions in isospin 0 that gives rise to the σ enhancement, and the strong attraction in isospin 1 that corresponds to the relatively narrow ρ resonance. As shown by Lüscher [27], taking account of hadron interactions, the finite-volume energy spectrum will be modified with respect to Eq. (5). The modification (at least

---

[6]We are neglecting small discretization effects in the dispersion relation.
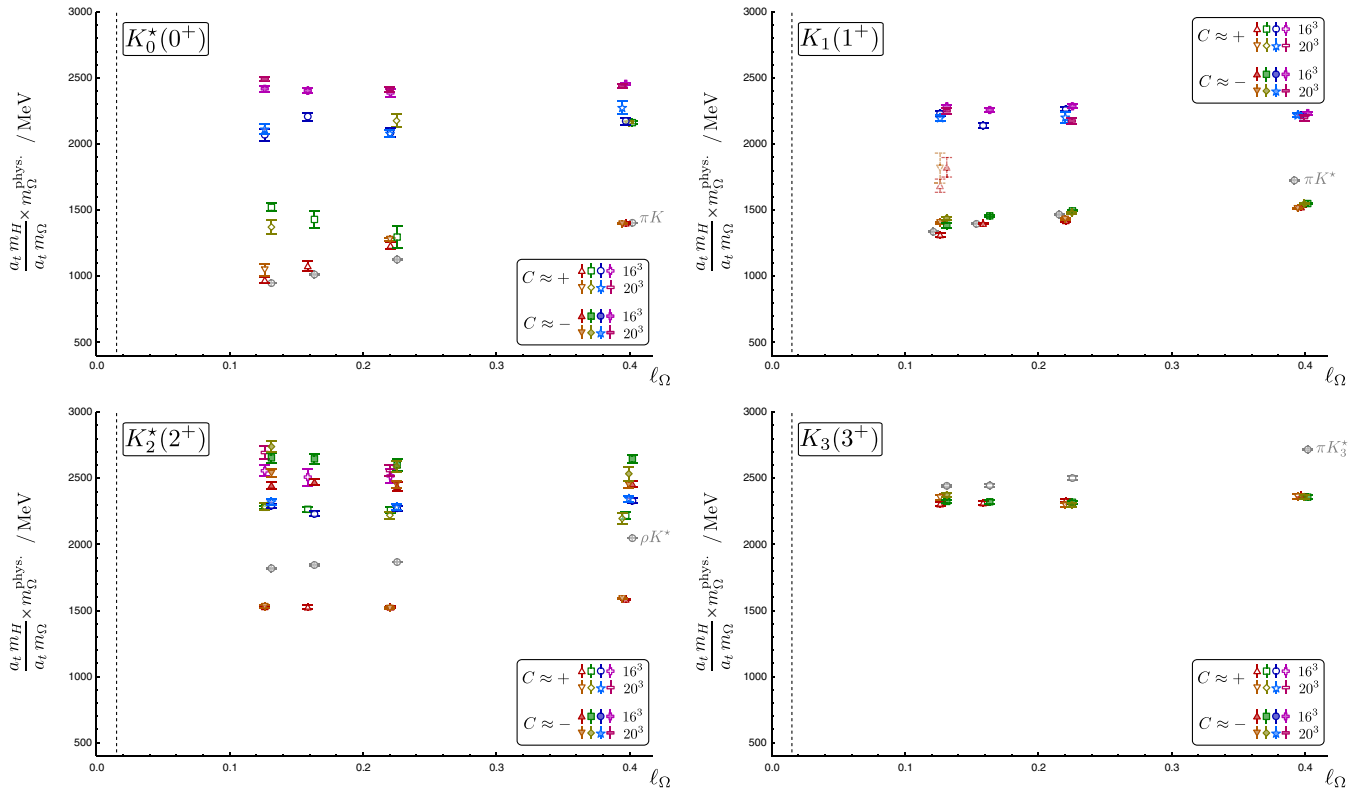
FIG. 22 (color online).   Lightest positive parity kaons. Hollow (filled) symbols indicate dominance of $C = +(-)$.

in the elastic case) can be related to the hadron-hadron scattering phase shift which encodes details of attractive or repulsive interactions and even of resonant behavior.

A simple schematic framework in which to view the finite-volume eigenstates is in terms of admixtures of idealized noninteracting basis states. For example, at low-energy in the T_1^{--} channel, one might consider there to be a space of noninteracting pion-pair states with the various relative momenta allowed in a finite cubic box. In addition, we can allow a space of single-hadron vector bound states like the ρ, which we assume to be localized to a region of space somewhat smaller than the size of the

lattice box. The pion-pair state energies vary rapidly with changing box-size while the "ρ" bound-states would be essentially volume-independent for volumes larger than the size of the bound-states. If one supplies a resonant phase-shift (such as the ρ in $\pi\pi$ scattering), Lüscher's formulas give rise to avoided level crossings as a function of lattice size that resemble the behavior of approximate eigenstates within time-independent quantum mechanical perturbation theory. The finite-volume eigenstates can be viewed then as admixtures of the "ρ" bound-states and the pion-pair states where the degree of mixing is determined by the phase-shift and the volume of the box.
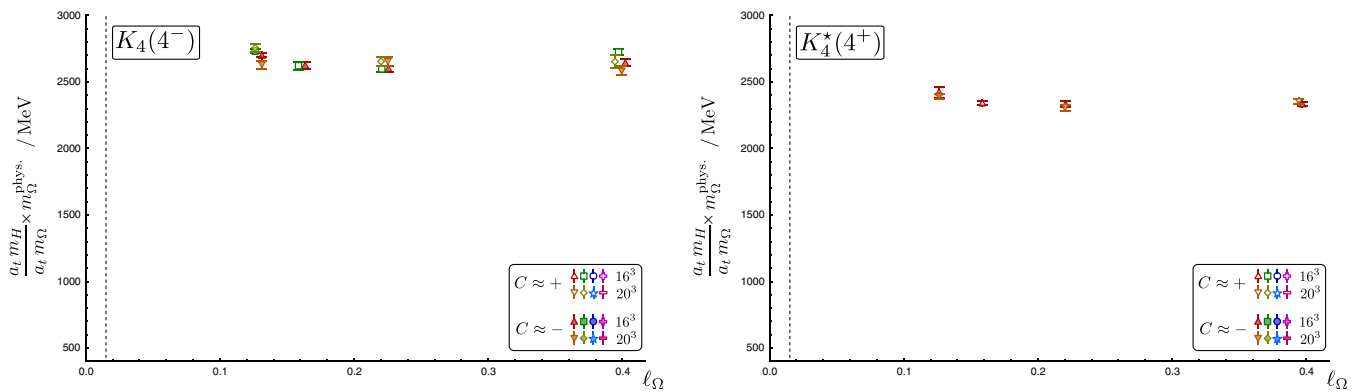

FIG. 23 (color online).   Lightest spin-4 kaons. Hollow (filled) symbols indicate dominance of $C = +(-)$.
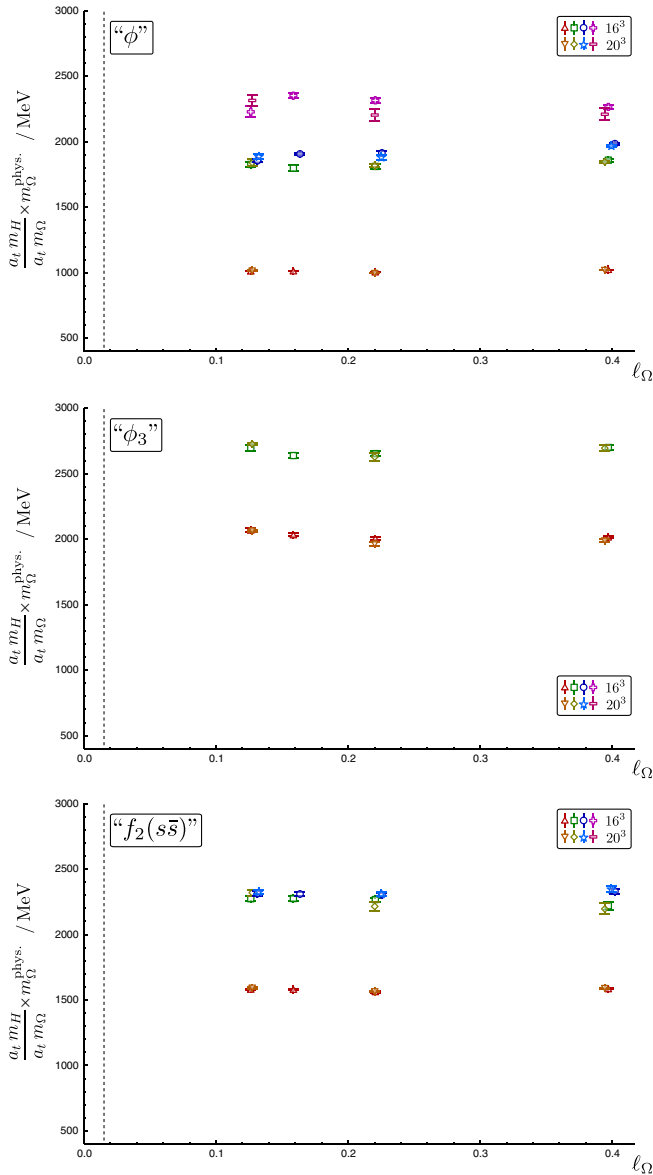
FIG. 24 (color online). Lightest "strangeonium" states with $J^{PC} = 1^{--}, 3^{--}, 2^{++}$.

In Figs. 25 and 26 we show the extracted *743* spectrum superimposed with the positions of *noninteracting* meson-meson states for 16^3 and 20^3 lattices. The distribution across irreps is determined using the "in-flight" cubic symmetry group theory tables from [45,46]. We show only pairs of $SU(3)_F$ octet states (since we have not determined the masses of the singlets or any other possible multiplets) and do not indicate the multiplicity of flavored states for each level (which follows from the $SU(3)$ Clebsch-Gordan series for $\mathbf{8} \otimes \mathbf{8} \to \mathbf{8}$).

What is clear from Figs. 25 and 26, is that the extracted spectrum does not seem to be related in any obvious way to the noninteracting two-particle spectrum. The distribution of two-particle states across different irreps is determined not by the cubic symmetry of our discretized lattice, but
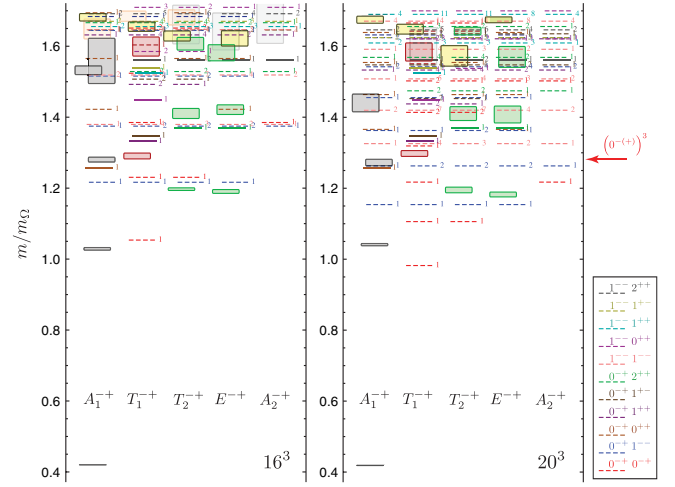

FIG. 25 (color online). *743* spectrum on 16^3 and 20^3 lattices. Boxes show the extracted Λ^{-+} spectrum. Lines are the non-interacting two-meson state positions estimated from Eq. (5) and the tables of [45,46] (solid lines at $\vec{p} = (000)$), the small numbers indicate the multiplicity. Additional flavor multiplicity not shown. Also shown is the position of the lowest three-meson threshold.

rather by the spatial momenta allowed by the boundary conditions on the cubic volume in which we are performing our calculations. We have seen that the observed spectrum split across the different irreducible representations conforms to that expected for single-particle states, with only negligible effects from cubic symmetry on the scale a_s. In contrast, the pattern across different irreps expected for multiparticle states would be quite different. This leads further credence to our assertion that two-particle states are contributing little to the calculated correlators.

How can we explain the lack of two-meson states in the spectrum we observe? Clearly, the basis set of operators employed has a very small overlap with states that pre-
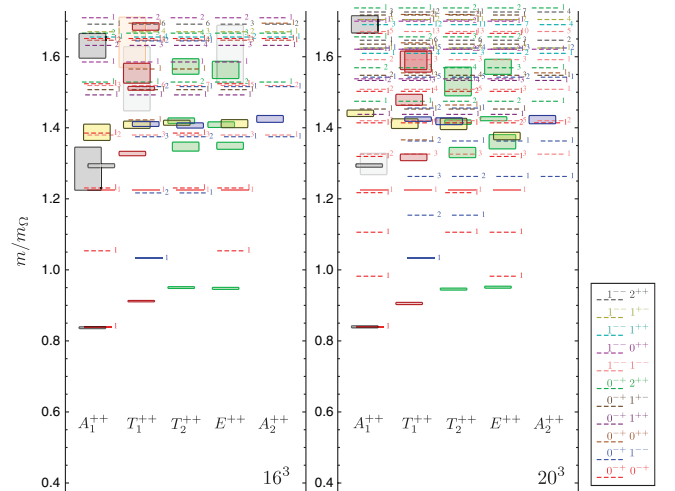

FIG. 26 (color online). As Fig. 25 for Λ^{++}.

dominantly resemble a composite of two mesons with well-defined and opposite momentum. This small overlap means the contribution to the correlation function coming from the significant number of two-meson states is not resolved within the statistical precision of our calculation.

This effect has been observed before in other dynamical-quark Monte Carlo measurements [47,48] of the energies of states that are above threshold, although perhaps not to the dramatic degree seen in this study. One cause of this suppression may come directly from confinement dynamics of strongly interacting gluons. The interquark gluon flux shows considerable reluctance to break in the regime where it is energetically favorable to form two well-separated color singlets. This has been seen [49,50] as a very small overlap of an operator comprising a gluonic string onto the ground state of this system.

The overlap of a localized quark-bilinear operator onto a two-meson state will be suppressed by $1/\sqrt{V}$, where V is the lattice volume, if the operator creates a resonance with a finite width in the infinite volume limit. This falloff is matched by a growth in the density of states with the volume, and the resonant state thus maintains a finite width as the mixing with each discrete state falls. The simulations in this study are carried out in cubic volumes with side lengths bigger than 2 fm, which might be sufficiently large that the mixing between one of the low-lying–two-particle states and a resonance is suppressed sufficiently for it to be undetectable with the quark-bilinear operator basis.

Even if the mixing between localized single-hadron states and two-meson states to form resonancelike finite-volume eigenstates is not small, there still remains a practical difficulty associated with using only quark-bilinear operators. In this case, the state can be produced at the source time slice through its localized single-hadron component, while the correlator time dependence obtained from e^{-Ht} will indicate the mass of the resonant eigenstate. Consider a hypothetical situation in which a single two-meson state, denoted by $|2\rangle$, mixes arbitrarily strongly with a single localized single-hadron state, $|1\rangle$, with all other states being sufficiently distant in energy as to be negligible. There will be two eigenstates

$$|\mathfrak{a}\rangle = \cos\theta|1\rangle + \sin\theta|2\rangle \qquad |\mathfrak{b}\rangle = -\sin\theta|1\rangle + \cos\theta|2\rangle,$$

with masses $m_{\mathfrak{a}}$, $m_{\mathfrak{b}}$. At the source (and sink), only the localized single-hadron component of each state overlaps with the operators in our basis and hence the overlaps, $Z_i^{\mathfrak{a},\mathfrak{b}} \equiv \langle \mathfrak{a}, \mathfrak{b}|\mathcal{O}_i|0\rangle$, will differ only by an overall multiplicative constant, $Z_i^{\mathfrak{a}} = \cos\theta Z_i^{|1\rangle}$, $Z_i^{\mathfrak{b}} = -\sin\theta Z_i^{|1\rangle}$. As such, the eigenvectors $v^{\mathfrak{a}}$, $v^{\mathfrak{b}}$ point in the same direction and cannot be made orthogonal. Thus, the time dependence of both states will appear in the *same* principal correlator as

$$\lambda(t) \sim A_{\mathfrak{a}}e^{-m_{\mathfrak{a}}(t-t_0)} + A_{\mathfrak{b}}e^{-m_{\mathfrak{b}}(t-t_0)} + \ldots$$

Since $m_{\mathfrak{a}}$ and $m_{\mathfrak{b}}$ most likely do not differ significantly (on the scale of a_t^{-1}), it will prove very difficult to extract a

clear signal of two-exponential behavior from the principal correlator. This is precisely why the variational method's orthogonality condition on near degenerate states is so useful, but we see that it cannot work here and we are left trying to extract two nearby states from a χ^2 fit to time dependence. Typically this is not possible and reasonable looking fits to data are obtained with just one low-mass exponential.

If this is what is occurring in parts of our extracted spectrum, that we are extracting states which are admixtures of "single-particle" and multimeson states, but that we are not extracting the orthogonal mixtures, how should we interpret the mass values we are extracting? One conservative approach would be to suggest that our mass values are accurate only up to the hadronic width of the state extracted, since this width is correlated with mixing with multimeson states via the scattering phase shift.

We would like to explicitly observe resonant behavior of states in our calculations and as such we must countenance the inclusion in our operator basis of operators with larger numbers of fermion fields in order to obtain healthy overlap with multihadron states. This can be done while respecting the lattice symmetries using the tables in [45,46]. By using single-meson operators subduced into the "in flight" little-group irreps from operators of definite continuum helicity, it may prove possible to utilize something similar to the spin identification carried out in this paper. These constructions are underway, and distillation, with the possible use of a stochastic estimator [38], affords an efficient numerical means of implementing them [32].

X. SUMMARY

We have described in some detail our method for extracting a large number of excited states using dynamical anisotropic lattices, distillation technology and a variational analysis with an extensive basis of carefully constructed operators. We have demonstrated the stability of the spectra with respect to changing the specific set of meson operators used, the number of distillation vectors and the details of the variational analysis. Our method of spin identification based on operator overlaps has enabled us to confidently assign continuum spin to many states.

We have successfully applied these techniques for two volumes on multiple mass sets: one with three degenerate flavors of quark (*743*) and three with lighter u and d quarks giving mild breaking of $SU(3)_F$ and pion masses down to $\sim$400 MeV. In all cases, we see mostly no significant volume dependence. On all mass sets and volumes, we are able to reliably extract a large number of excited states with all PC combinations, states with high spin, up to and including spin four (4^{++}, 4^{-+} and 4^{--}), and states with exotic quantum numbers (0^{+-}, 1^{-+} and 2^{+-}). The exotic states are particularly interesting and their presence points to the influence of explicit gluonic degrees-of-freedom. In Fig. 27, we summarize our results on exotic states and
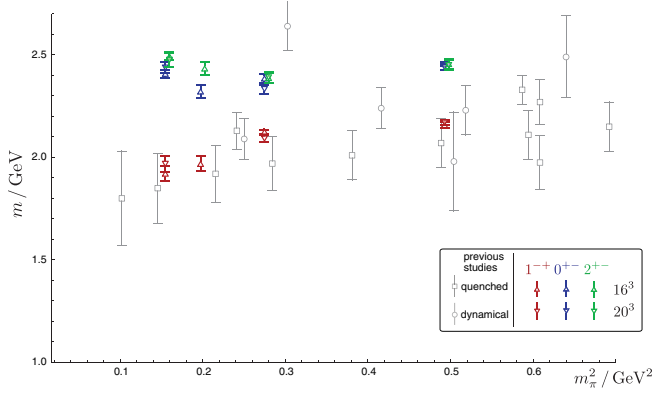
FIG. 27 (color online). Summary of extracted isovector exotic states. For comparison 1^{-+} results from Refs. [21–26] are also plotted.

compare with previous lattice QCD results from Refs. [21–26].

The extracted spectra show features of the $n^{2S+1}L_J$ state assignment of bound-state quark models, along with states (both exotic and nonexotic) which do not seem to lie within that classification. A detailed model-dependent interpretation of these spectra is called for, comparing overlaps with quark-model expectations and determining the degree of mixing of nonexotic hybrids and quark-model states. This work is ongoing.

We have presented kaon spectra and observe little or no mixing between the two charge-conjugation eigenstates ($C = +$ and $C = -$); the resulting spectrum largely corresponds to the superposition of the $C = -$ and $C = +$ isovector spectra modulo the mass shift due to the light-quark—strange-quark mass difference. In the $SU(3)_F$ limit, there can be no such mixing and on the mass sets considered we are still rather close to this limit ($1 \leq m_K/m_\pi \leq 1.39$), so it is therefore not surprising that the mixing is small. Of particular interest at lighter quark masses, closer to the physical $m_K/m_\pi = 3.5$, will be the mixing between the axial kaons, $K_1(1270)$ and $K_1(1400)$, which, using a combination of experiment and models [43,44], is expected to be large.

We have argued that we see little evidence for two-particle states in our spectra and that to study such states we need to construct operators with a larger number of fermion fields. Such constructions are in progress and we believe that the addition of these operators will lead to a denser spectrum of states which can be interpreted in terms of resonances via techniques like Lüscher's and its inelastic extensions.

With the excited state spectra extracted herein, we argue that it does not make sense to attempt chiral extrapolation given that we cannot form a clear field-theoretic interpretation of the extracted energy levels. Once we have a handle on the two-meson levels, we can apply the techniques mentioned above to extract something like a phase shift, or more generally elements of the S-matrix, at dis-

crete energy values. The phase shift may show resonant behavior, which can be fitted with, in the simplest case, a Breit-Wigner form. The mass and width parameters of this Breit-Wigner are quantities which should be more amenable to chiral extrapolation.

A further avenue of study is the computation of disconnected two-point correlators giving access to isoscalar mesons; here we are interested in determining how QCD decides to mix light and strange. In addition, methods similar to those detailed in this paper are being applied in the baryon sector where the lattice irrep spectrum suffers from an even greater degree of degeneracy. An important aim of the Hadron Spectrum Collaboration is the calculation of light meson photocouplings which are relevant for, amongst other things, the GlueX experiment at the JLab 12 GeV upgrade where light mesons will be studied in photoproduction, with particular interest in exotics.

APPENDIX A: SUBDUCTION COEFFICIENTS

Here we give a derivation of the subduction coefficients before listing their explicit values for all integer spins up to $J = 4$. An alternative derivation using the group-theoretic projection formula is also described.

The continuum spin J is reducible under the group of lattice rotations (the octahedral group or equivalently the cubic group). We use "subduction" coefficients to project the continuum based operators onto their suitable octahedral group based versions via

$$\mathcal{O}^{[J]}_{\Lambda,\lambda} = \sum_M \mathcal{S}^{J,M}_{\Lambda,\lambda} \mathcal{O}^{J,M}, \qquad (A1)$$

where $\mathcal{O}^{J,M}$ are the continuum operators with some definite total spin J and spin component M. For each $J \rightarrow \Lambda$, there is a matrix in the values of M and the rows of the irrep, λ, that performs this mapping, i.e., the subduction coefficients, $\mathcal{S}^{J,M}_{\Lambda,\lambda}$.

As shown in Table III, the $J = 0$ continuum spin sub-duces only onto the one-dimensional A_1 irrep and so trivially we have $\mathcal{S}^{0,0}_{A_1,1} = 1$. The simplest nontrivial subduction is that of continuum $J = 1$ into the T_1 irrep and this is given by

λ $\backslash$ ^{M}	$(J = 1) \to T_1$		
	1	0	-1
1	1	0	0
2	0	1	0
3	0	0	1

where the T_1 is a faithful representation of $J = 1$ (The basis used here follows Ref. [2]).

The subduction coefficients for higher spins can be built up using continuum and octahedral group Clebsch-Gordan coefficients using

$$S^{J,M}_{\Lambda,\lambda} = N \sum_{\lambda_1,\lambda_2} \sum_{m_1,m_2} C\begin{pmatrix} \Lambda & \Lambda_1 & \Lambda_2 \\ \lambda & \lambda_1 & \lambda_2 \end{pmatrix}$$
$$\times S^{J_1,m_1}_{\Lambda_1,\lambda_1} S^{J_2,m_2}_{\Lambda_2,\lambda_2} \langle J_1, m_1; J_2, m_2 | J, M \rangle. \quad (A2)$$

Here $\langle J_1, M_1; J_2, M_2 | J, M \rangle$ is the usual $SO(3)$ Clebsch-Gordan coefficient for $J_1 \otimes J_2 \to J$ and

$$C\begin{pmatrix} \Lambda & \Lambda_1 & \Lambda_2 \\ \lambda & \lambda_1 & \lambda_2 \end{pmatrix}$$

is the octahedral group Clebsch-Gordan coefficient for $\Lambda_1 \otimes \Lambda_2 \to \Lambda$. N is a normalization factor, fixed by the requirement that the subduction coefficients form an orthogonal matrix, $\sum_M \mathcal{S}^{J,M}_{\Lambda,\lambda} \mathcal{S}^{J,M*}_{\Lambda',\lambda'} = \delta_{\Lambda,\Lambda'} \delta_{\lambda,\lambda'}$.

This iteration formula can be constructed by noting that, for appropriately normalized states, $\mathcal{S}^{J,M}_{\Lambda,\lambda} = \langle \Lambda, \lambda | J, M \rangle$ and so

$$\mathcal{S}^{J,M}_{\Lambda,\lambda} = N \sum_{\lambda_1,\lambda_2} \sum_{m_1,m_2} \langle \Lambda, \lambda | \Lambda_1, \lambda_1; \Lambda_2, \lambda_2 \rangle$$
$$\times \langle \Lambda_1, \lambda_1; \Lambda_2, \lambda_2 | J_1, m_1; J_2, m_2 \rangle$$
$$\times \langle J_1, m_1; J_2, m_2 | J, M \rangle. \quad (A3)$$

Substituting for the continuum and octahedral group Clebsch-Gordan coefficients and $\langle \Lambda_1, \lambda_1; \Lambda_2, \lambda_2 | J_1, m_1; J_2, m_2 \rangle = \langle \Lambda_1, \lambda_1 | J_1, m_1 \rangle \langle \Lambda_2, \lambda_2 | J_2, m_2 \rangle = \mathcal{S}^{J_1,m_1}_{\Lambda_1,\lambda_1} \mathcal{S}^{J_2,m_2}_{\Lambda_2,\lambda_2}$ gives the result in Eq. (A2).

For $J = 2$ to $J = 4$, the subduction coefficients are shown below:

λ $\backslash$ ^{M}	$(J = 2) \to T_2$				
	2	1	0	-1	-2
1	0	1	0	0	0
2	$\frac{1}{\sqrt{2}}$	0	0	0	$-\frac{1}{\sqrt{2}}$
3	0	0	0	1	0

λ $\backslash$ ^{M}	$(J = 2) \to E$				
	2	1	0	-1	-2
1	0	0	1	0	0
2	$\frac{1}{\sqrt{2}}$	0	0	0	$\frac{1}{\sqrt{2}}$

λ $\backslash$ ^{M}	$(J = 3) \to T_1$						
	3	2	1	0	-1	-2	-3
1	0	0	$\sqrt{\frac{3}{8}}$	0	0	0	$\sqrt{\frac{5}{8}}$
2	0	0	0	-1	0	0	0
3	$\sqrt{\frac{5}{8}}$	0	0	0	$\sqrt{\frac{3}{8}}$	0	0

λ $\backslash$ ^{M}	$(J = 3) \to T_2$						
	3	2	1	0	-1	-2	-3
1	0	0	$\sqrt{\frac{5}{8}}$	0	0	0	$-\sqrt{\frac{3}{8}}$
2	0	$-\frac{1}{\sqrt{2}}$	0	0	0	$-\frac{1}{\sqrt{2}}$	0
3	$\sqrt{\frac{3}{8}}$	0	0	0	$-\sqrt{\frac{5}{8}}$	0	0

λ $\backslash$ ^{M}	$(J = 3) \to A_2$						
	3	2	1	0	-1	-2	-3
1	0	$\frac{1}{\sqrt{2}}$	0	0	0	$-\frac{1}{\sqrt{2}}$	0

λ $\backslash$ ^{M}	$(J = 4) \to A_1$								
	4	3	2	1	0	-1	-2	-3	-4
1	$\sqrt{\frac{5}{24}}$	0	0	0	$\sqrt{\frac{7}{12}}$	0	0	0	$\sqrt{\frac{5}{24}}$

λ $\backslash$ ^{M}	$(J = 4) \to T_1$								
	4	3	2	1	0	-1	-2	-3	-4
1	0	0	0	$-\sqrt{\frac{7}{8}}$	0	0	0	$-\frac{1}{\sqrt{8}}$	0
2	$\frac{1}{\sqrt{2}}$	0	0	0	0	0	0	0	$-\frac{1}{\sqrt{2}}$
3	0	$\frac{1}{\sqrt{8}}$	0	0	0	$\sqrt{\frac{7}{8}}$	0	0	0

λ $\backslash$ ^{M}	$(J = 4) \to T_2$								
	4	3	2	1	0	-1	-2	-3	-4
1	0	0	0	$-\frac{1}{\sqrt{8}}$	0	0	0	$\sqrt{\frac{7}{8}}$	0
2	0	0	$\frac{1}{\sqrt{2}}$	0	0	0	$-\frac{1}{\sqrt{2}}$	0	0
3	0	$\sqrt{\frac{7}{8}}$	0	0	0	$-\frac{1}{\sqrt{8}}$	0	0	0

λ $\backslash$ ^{M}	$(J = 4) \to E$								
	4	3	2	1	0	-1	-2	-3	-4
1	$\sqrt{\frac{7}{24}}$	0	0	0	$-\sqrt{\frac{5}{12}}$	0	0	0	$\sqrt{\frac{7}{24}}$
2	0	0	$\frac{1}{\sqrt{2}}$	0	0	0	$\frac{1}{\sqrt{2}}$	0	0

An alternative method for constructing the subduction coefficients is by using the group-theoretic projection formula:

$$\mathcal{O}^{[J]}_{\Lambda,\lambda} = \frac{d_\Lambda}{g_G} \sum_{R \in G} \Gamma^\Lambda_{\lambda,\mu}(R) \sum_{M'} R_{MM'} \mathcal{O}^{J,M'}, \quad (A4)$$

where G is the octahedral group, g_G is the order of the group G (i.e., 24), d_Λ is the dimension of octahedral group irrep Λ, $R_{MM'}$ is an element of G acting on $\mathcal{O}^{J,M'}$, and $\Gamma^\Lambda_{\lambda,\mu}(R)$ is the representation of R in Λ. Here the operators

$\mathcal{O}^{J,M'}$ have definite spin and so $R_{MM'} = D^{(J)}_{M'M}(R)$ (a Wigner-D matrix). The $\Gamma^\Lambda_{\lambda,\mu}(R)$ are found, for example, by considering a basis for the irreps in terms of spherical harmonics [2] and then using the transformation properties of spherical harmonics under rotations. Once all possible

operators $\mathcal{O}^{[J]}_{\Lambda,\lambda}$ have been found (considering all M and μ), the linearly independent combinations are constructed. These combinations then give the subduction coefficients which are identical, up to possible phases and choice of basis, to those obtained using the method described above.

[1] S. Basak *et al.*, Phys. Rev. D **72**, 094506 (2005).
[2] S. Basak *et al.* (Lattice Hadron Physics (LHPC)), Phys. Rev. D **72**, 074501 (2005).
[3] S. Basak *et al.*, Phys. Rev. D **76**, 074504 (2007).
[4] J. M. Bulava *et al.*, Phys. Rev. D **79**, 034505 (2009).
[5] J. J. Dudek, R. G. Edwards, N. Mathur, and D. G. Richards, Phys. Rev. D **77**, 034501 (2008).
[6] J. J. Dudek, R. G. Edwards, and D. G. Richards, Phys. Rev. D **73**, 074507 (2006).
[7] J. J. Dudek, R. Edwards, and C. E. Thomas, Phys. Rev. D **79**, 094504 (2009).
[8] J. J. Dudek, R. G. Edwards, M. J. Peardon, D. G. Richards, and C. E. Thomas, Phys. Rev. Lett. **103**, 262001 (2009).
[9] C. Aubin *et al.*, Phys. Rev. D **70**, 094505 (2004).
[10] T. Burch *et al.*, Phys. Rev. D **81**, 034508 (2010).
[11] K. Jansen, C. McNeile, C. Michael, C. Urbach, and (f. t. E. Collaboration), Phys. Rev. D **80**, 054510 (2009).
[12] A. Walker-Loud *et al.*, Phys. Rev. D **79**, 054502 (2009).
[13] T. Burch, C. Hagen, M. Hetzenegger, and A. Schafer, Phys. Rev. D **79**, 114503 (2009).
[14] R. G. Petry, D. Harnett, R. Lewis, and R. M. Woloshyn, Phys. Rev. D **78**, 074502 (2008).
[15] C. Gattringer, L. Y. Glozman, C. B. Lang, D. Mohler, and S. Prelovsek, Phys. Rev. D **78**, 034501 (2008).
[16] T. Burch *et al.*, Phys. Rev. D **73**, 094505 (2006).
[17] T. Burch *et al.* (Bern-Graz-Regensburg), Phys. Rev. D **70**, 054502 (2004).
[18] P. Lacock, C. Michael, P. Boyle, and P. Rowland (UKQCD), Phys. Rev. D **54**, 6997 (1996).
[19] T. Yamazaki *et al.* (CP-PACS), Phys. Rev. D **65**, 014501 (2001).
[20] M. Peardon *et al.* (Hadron Spectrum), Phys. Rev. D **80**, 054506 (2009).
[21] C. Bernard *et al.*, Phys. Rev. D **68**, 074505 (2003).
[22] C. W. Bernard *et al.* (MILC), Phys. Rev. D **56**, 7039 (1997).
[23] P. Lacock and K. Schilling (TXL), Nucl. Phys. B, Proc. Suppl. **73**, 261 (1999).
[24] P. Lacock, C. Michael, P. Boyle, and P. Rowland (UKQCD), Phys. Lett. B **401**, 308 (1997).
[25] C. McNeile and C. Michael (UKQCD), Phys. Rev. D **73**, 074506 (2006).
[26] J. N. Hedditch *et al.*, Phys. Rev. D **72**, 114507 (2005).
[27] M. Lüscher, Nucl. Phys. **B364**, 237 (1991).
[28] R. G. Edwards, B. Joo, and H.-W. Lin, Phys. Rev. D **78**, 054501 (2008).
[29] H.-W. Lin *et al.* (Hadron Spectrum), Phys. Rev. D **79**, 034502 (2009).
[30] C. R. Allton *et al.* (UKQCD), Phys. Rev. D **47**, 5128 (1993).
[31] C. Morningstar and M. J. Peardon, Phys. Rev. D **69**, 054501 (2004).
[32] J. Foley *et al.*, arXiv:1003.2154.
[33] C. Michael, Nucl. Phys. **B259**, 58 (1985).
[34] M. Luscher and U. Wolff, Nucl. Phys. **B339**, 222 (1990).
[35] B. Blossier, M. Della Morte, G. Von Hippel, T. Mendes, and R. Sommer, J. High Energy Phys. 04 (2009) 094.
[36] J. J. Dudek and C. E. Thomas (Hadron Spectrum Collaboration), RECONFIT2 *package within* ADAT, git://git.jlab.org/pub/lattice/usqcd/adat.git.
[37] C. J. Morningstar and M. J. Peardon, Phys. Rev. D **60**, 034509 (1999).
[38] C. Morningstar *et al.*, arXiv:1002.0818.
[39] S. Godfrey and N. Isgur, Phys. Rev. D **32**, 189 (1985).
[40] N. Isgur and J. E. Paton, Phys. Rev. D **31**, 2910 (1985).
[41] J. J. Dudek and E. Rrapaj, Phys. Rev. D **78**, 094504 (2008).
[42] C. Amsler *et al.* (Particle Data Group), Phys. Lett. B **667**, 1 (2008).
[43] D. M. Asner *et al.* (CLEO), Phys. Rev. D **62**, 072006 (2000).
[44] T. Barnes, N. Black, and P. R. Page, Phys. Rev. D **68**, 054014 (2003).
[45] D. C. Moore and G. T. Fleming, Phys. Rev. D **73**, 014504 (2006).
[46] D. C. Moore and G. T. Fleming, Phys. Rev. D **74**, 054504 (2006).
[47] C. McNeile and C. Michael (UKQCD), Phys. Lett. B **556**, 177 (2003).
[48] S. Durr *et al.*, Science **322**, 1224 (2008).
[49] G. S. Bali, H. Neff, T. Duessel, T. Lippert, and K. Schilling (SESAM), Phys. Rev. D **71**, 114513 (2005).
[50] C. McNeile, C. Michael, and P. Pennanen (UKQCD), Phys. Rev. D **65**, 094505 (2002).
[51] M. A. Clark, R. Babich, K. Barros, R. C. Brower, and C. Rebbi, arXiv:0911.3191.
[52] R. G. Edwards and B. Joo (SciDAC Collaboration), Nucl. Phys. B, Proc. Suppl. **140**, 832 (2005).